TECHNICAL UNIVERSITY OF LIBEREC
Faculty of Textile Engineering

Carbon coating to impart electrical conductivity to textile material

Master Thesis

Study programme:	N0723A270002 Textile Engineering
Author:	**Divan Coetzee, B.Sc.**
Thesis Supervisors:	prof. Ing. Jakub Wiener, Ph.D. Department of material engineering

Liberec 2022

TECHNICAL UNIVERSITY OF LIBEREC
Faculty of Textile Engineering

Master Thesis Assignment Form

Carbon coating to impart electrical conductivity to textile material

Name and surname:	**Divan Coetzee, B.Sc.**
Identification number:	T19000378
Study programme:	N0723A270002 Textile Engineering
Assigning department:	Department of Nonwovens and Nanofibrous materials
Academic year:	**2020/2021**

Rules for Elaboration:

1. Perform a literature search on carbon-based materials for electrical coating purposes.
2. Develop a coating using selected carbon particles.
3. Find and use a suitable method for aplication of the developed carbon coatingon chosen textile.
4. Characterize the electrical properties of the carbon coated textile.
5. Discuss possible applications of the carbon coated material.

Scope of Graphic Work:	
Scope of Report:	40-60
Thesis Form:	printed/electronic
Thesis Language:	English

List of Specialised Literature:

1. CHUNG, D. D.L. Review: Graphite. Journal of Materials Science [online]. 2002, 37(8), 1475–1489. ISSN 00222461. Dostupné z: doi:10.1023/A:1014915307738

Thesis Supervisors:	prof. Ing. Jakub Wiener, Ph.D. Department of material engineering
Date of Thesis Assignment:	November 1, 2020
Date of Thesis Submission:	May 16, 2022

L.S.

doc. Ing. Vladimír Bajzík, Ph.D.
Dean

doc. Ing. Jiří Chvojka, Ph.D.
Head of Department

Liberec November 1, 2020

Declaration

I hereby certify, I, myself, have written my master thesis as an original and primary work using the literature listed below and consulting it with my thesis supervisor and my thesis counsellor.

I acknowledge that my master thesis is fully governed by Act No. 121/2000 Coll., the Copyright Act, in particular Article 60 – School Work.

I acknowledge that the Technical University of Liberec does not infringe my copyrights by using my master thesis for internal purposes of the Technical University of Liberec.

I am aware of my obligation to inform the Technical University of Liberec on having used or granted license to use the results of my master thesis; in such a case the Technical University of Liberec may require reimbursement of the costs incurred for creating the result up to their actual amount.

At the same time, I honestly declare that the text of the printed version of my master thesis is identical with the text of the electronic version uploaded into the IS/STAG.

I acknowledge that the Technical University of Liberec will make my master thesis public in accordance with paragraph 47b of Act No. 111/1998 Coll., on Higher Education Institutions and on Amendment to Other Acts (the Higher Education Act), as amended.

I am aware of the consequences which may under the Higher Education Act result from a breach of this declaration.

May 11, 2022

Divan Coetzee, B.Sc.

Acknowledgement

I thank my supervisors Prof. Ing. Jakub Wiener Ph.D. and Ing. Josef Večerník CSc. for their mentorship in the making of this thesis given all the difficulties and delays caused by the COVID pandemic. I also thank prof. Jiří Militký, CSc. for his guidance. To my colleagues and superiors, I say thank you for your assistance and advice where needed.

To my parents Pieter and Trudie Coetzee: none of my academic accomplishments would have been possible without your love and support. I am forever grateful.

Abstrakt

Byl vyvinut epoxidový/PEI/uhlíkový povlak obsahující různé množství grafenu nebo grafitu, který dodává netkané viskózové textilii elektrickou vodivost. Bylo zjištěno, že zvýšení obsahu uhlíkového plniva vede ke zvýšení elektrické vodivosti a že vícenásobné povlaky elektrickou vodivost dále zlepšují. Povrchově aktivní látka decilglukosid zlepšila promíchání částic, aniž by ovlivnila elektrickou vodivost. Potažený materiál vykazoval minimální elektrický odpor v rozsahu megaohmů, což z něj činí relativně slabý elektrický vodič, který však lze považovat za antistatický. Vzorky nevykazovaly žádné stínění EMI v rozsahu 30 MHz - 3 GHz.

Klíčová slova: polyethylenimin, epoxid 200, grafen, grafit, viskóza, elektrická vodivost, elektrický odpor

Abstract

An epoxy/PEI/carbon coating was developed containing differing amounts of graphene or graphite to impart electrical conductivity onto a nonwoven viscose textile. It was found that an increase in carbon filler content resulted in increased electrical conductivity and that multiple coatings improved electrical conductivity further. Decyl glucoside surfactant improved particle mixing without influencing electrical conductivity. The coated material exhibited a minimum electrical resistivity in the megaohm range which makes it a relatively weak electrical conductor, however it can be considered as antistatic. The samples indicated no EMI shielding in the 30 MHz – 3 GHz range.

Keywords: polyethyleneimine, epoxy 200, graphene, graphite, viscose, electrical conductivity, electrical resistance

List of Contents

List of figures

List of tables

List of abbreviations

BPO	Benzoyl Peroxide
CVD	Chemical Vapour Deposition
DOP	Dioctyl Phthalate
EMI	Electromagnetic Interference
GO	Graphene Oxide
HOPG	Highly Orientated Pyrolytic Graphite
IACS	International Annealed Copper Standard
PEI	Polyethyleneimine
PMMA	Poly(methylmethacrylate)
PVC	Poly(vinyl chloride)
RGO	Reduced Graphene Oxide
DSC	Differential Scanning Calorimetry
SEM	Scanning Electron Microscope
POM	Polarized Light Optical Microscope

List of symbols

Å	Angstrom
eV	Electron Volt
H	Hamiltonian
γ	Specific electric band
Γ	Total electric band energy
E	Energy level
v	Wave velocity
Δ	Total effective energy
σ	Electrical conductivity
μ	Electron mobility
l	Free electron path
K	Kelvin
ρs	Surface electrical resistivity
ρv	Volume electrical resistivity
Rs	Surface electrical resistance
Rv	Volume electrical resistance
°C	Degrees Celsius
mm	Millimetre
cm	Centimetre
Ω	Ohm
MΩ	Megaohm

1. Introduction

Carbon is the most abundant element in the biosphere with its pure form receiving increasing attention in recent years as academic emphasis is placed on nanotechnologies. It has proven useful for use in fields such as electrodes, energy storage, electro- and heterogeneous catalysis, purification, gas separation and CO_2 capture applications. The use of carbon nanomaterials has contributed to the awarding of several Nobel prizes in modern times. Most carbon-based materials are derived from fossil-based precursors which typically require harsh or energy intensive conditions such as when using electric arc discharge or chemical vapor deposition (CVD). This makes the process to produce carbon-based materials difficult to scale for industrial production making it expensive [1]. In many countries naturally occurring graphite is mined by either open pit or underground methods.

Carbon is a polymorphic material meaning it can form allotropes due to its valency. Pure carbon exists in three forms namely graphite, diamond and fullerites. Structural differences are attributed to the orbital overlap between the carbon atoms as illustrated in figure 1 [2–4]. Diamond exhibits a three-dimensional crystal structure of sp^3 hybridized carbon atoms resulting in a covalent network solid. Graphite consists of carbon layers referred to as graphene sheets which are stacked in an AB sequence different to that of the AB sequence in a hexagonal close packed structure. Carbon atoms in graphite layers are in a sp^2 hybridized trigonal planar form which produces a carbon network layer of single atom thickness. The graphene sheets in graphite are held together by weak van der Waals forces produced by delocalized π-orbitals in the structure. These forces are weak enough to allow the graphene sheets to slide over each other making graphite a good lubricant. Carbon materials may also exhibit an amorphous structure which are like graphite but does not contain the AB stacking sequence. The degree of crystallinity is increased with an increase in temperature. Graphite is anisotropic meaning it is an excellent electrical and thermal conductor within the graphene layers, but not perpendicular to it [5]. This is due to the weak van der Waals forces between the graphene layers [2]. The anisotropic nature of graphite enables it to undergo chemical reactions such as in the production of graphene oxide. This allows intercalating reagents to enter the space between the graphene layers allowing for chemical reactions to take place around it [2, 6].

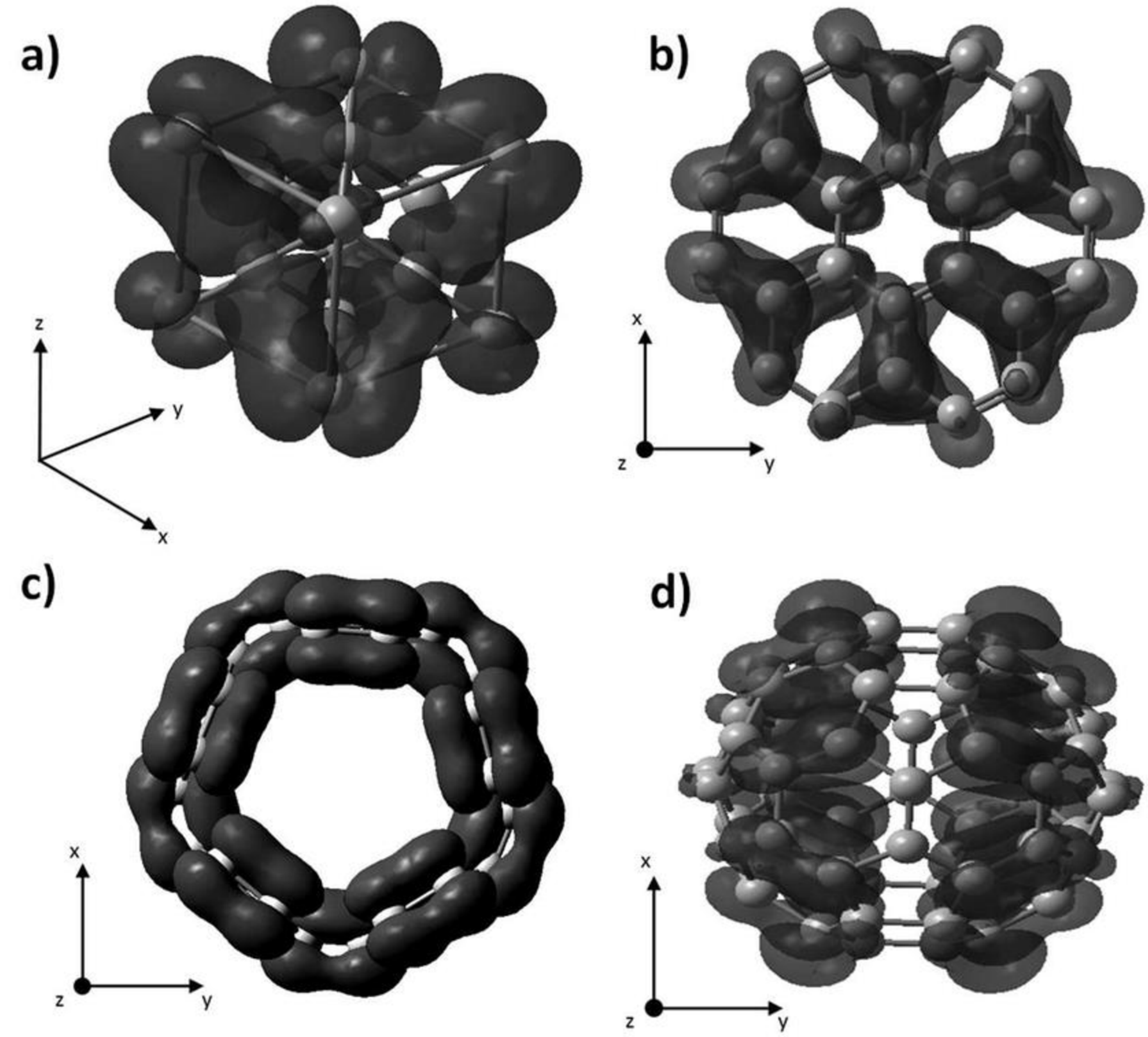

Figure 1: Molecular orbital for carbon based structures: a) diamond(sp^3), b) graphite(sp^2), c) SWCNT(sp^2) and d) fullerene(sp^2) Creative Commons License [3].

Composite conductivity, especially electrical conductivity, is related to the formation of conductive pathways inside the composite structure. The amount of filler required will depend on factors such as the kind of filler, aspect ratio, dispersion and distribution, surface treatment, orientation, and agglomeration, polymer type, phase structure, mixing method, surface energies until the percolation threshold is reached. The percolation threshold is when a critical volume of filler is reached in a composite at which enough inter particle contact occurs to form a network or conductive pathways. Before this point there are little pathways and thus conductivity is weak and beyond this point conductivity will plateau [7, 8].

To produce a coating which would not add significant weight to the textile material it was determined that the coating should have as low viscosity as possible to only coat the fibres. This would ensure to minimise the presence of excess coating solution on the material which could be successfully removed by vacuum or pressure. It was previously investigated that a

PEI/Epoxy 200 55V solution coated on a polyamide woven textile exhibited good mechanical properties whilst remaining relatively flexible [9]. It was therefore decided to modify this system by incorporating an electrically conductive component. For this purpose, a coating consisting of Epoxy 200 V55 and polyethyleneimine (PEI) was used since both are miscible in water which would be used to reduce the solution viscosity. Aliphatic, aromatic, and cycloaliphatic amines are common functional groups of composite hardeners. Highly branched PEI has been used more recently due to its ability to form crosslinks with epoxy and for its compatibility with carbon filler materials. Crosslinks are formed when the ester groups in the epoxy reacts with the primary and secondary amines of the PEI to form secondary and tertiary amines respectively [10, 11]. Graphene powder with a particle size of 20-30 µm was chosen as conductive filler. For comparison spherical graphite with dimensions ranging 1 – 3 µm was selected. Carbon particles are hydrophobic due to low surface energy which increases with decrease in particle size due to increased surface area. This results in the particles agglomerating and not mixing in aqueous solution [8, 12]. To overcome this problem of particle agglomeration non-ionic surfactant, decyl glucoside, was used in samples which exhibited this problem during preparation.

2. Carbon particle characterisation

2.1.Physical structure

The carbon atoms in the AB stacked layers of graphite are arranged in a hexagonal pattern which has a hexagonal unit cell length of c = 6.71 Å and a = 2.46 Å with 4 atoms per unit cell as illustrated in figure 2. The distinct atoms are labelled A, A', B and B' with A and B in one layer plane and A' and B' displaced by half the crystallographic c-axis of 3.35 Å. The crystal structure corresponds to the $P6_3/mmc$ space group. This states that the principal (P) unit cell possesses a mirror plane perpendicular to the c-axis as well as 3 mirror planes parallel to the c-axis and glide planes as indicated by the mmc designation. The $P6_3$ designation indicates a screw axis because of the AB stacking meaning that 6 rotational operations are required before a full rotation occurs along the rotational axis followed by a translation of 1/3 of the parallel lattice vector. A centre of inversion symmetry is located half way between atoms A and A' [2, 13–16].

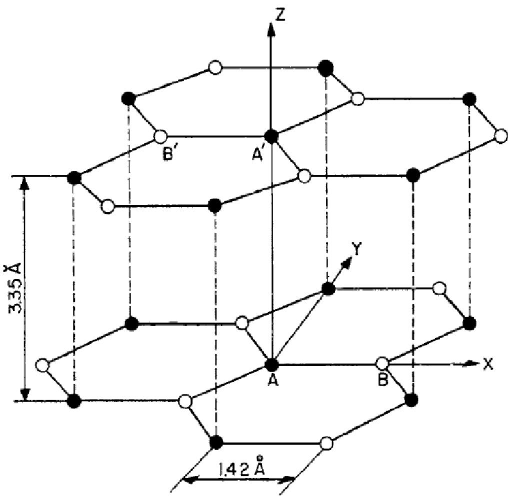

Figure 2: The crystal structure of graphite with four atoms per unit cell, namely A, A', B and B'. The atoms A and A', shown with full circles, have neighbours directly above and below in adjacent layer planes; the atoms B and B', shown with open circles, have neighbours directly above and below in layer planes 6.71 Å away [2].

The 2s and $2p_x$ and $2p_y$ orbitals in the graphite structure forms σ-bonding between the carbon atoms resulting in the sp^2 hybridized orbitals which are directed 120° apart on each layer plane. The delocalized orbital of the $2p_z$ electron results in the π-symmetry which is responsible for the stabilization of the in-plane carbon bonding. This delocalization of loosely bound π-electrons results in high electron mobility which plays a dominant role in the electrical conductivity of graphitic materials. The layers are bound by weak van der Waals forces in the c-direction resulting in the anisotropic structure [2, 17].

2.2. Electrical properties

The electrical conductivity of graphite can be explained by the electronic energy band structure of the material. Each carbon atom has 4 valence electrons resulting in a unit cell containing 4 carbon atoms resulting in a total of 16 energy bands. 12 of these energy bands are σ-bands and 4 are π-bands. The 12 σ-bands are split between bonding and antibonding orbitals which are separated by about 5 eV with the 2 strongly coupled bonding and antibonding π-orbital bands in between respectively. The amount of valence electrons present fills 8 of these energy bands and thus the Fermi level lies in the middle of the 4 π-bands. The overlap of the upper π-bands of 0.03 eV along the Brillouin zone edges makes graphite a semi-metal as illustrated in figure 3 [2].

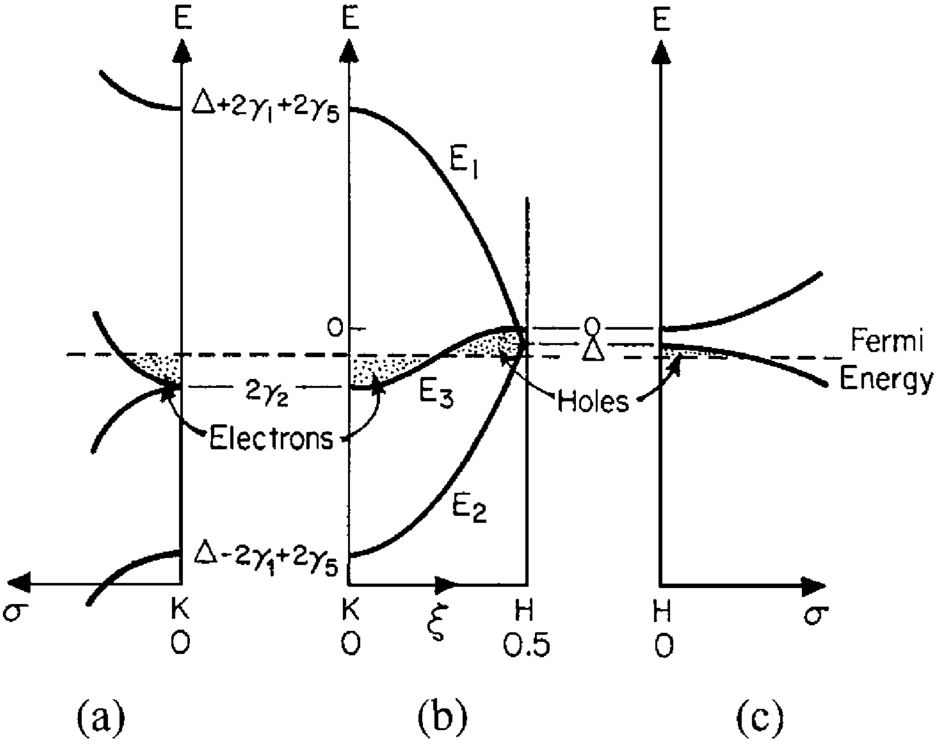

Figure 3: Three-dimensional energy bands of graphite, showing schematically the wave vector (ξ , σ) dependence of the energy (E) of the graphite π-bands. The dashed line represents the Fermi level (E° F) for pure graphite. (a) Energy vs dimensionless wave vector σ in the plane ξ =0 about the K-point. (b) Energy vs dimensionless wave vector ξ along the edges HKH and H'K'H'. (c) Energy vs σ in the plane ξ =1/2 about the H point [2].

An energy band model was developed by Slonczewski and Weiss to describe the electronic energy dispersion relations around the HKH axis in the Brillouin zone illustrated in figure 4. Fourier expansion in ξ was used to determine the energy dependence along the k_z direction. Due to weak interlayer binding the Fourier series converges. Perturbation theory

was used to expand the Hamiltonian in terms of *k*, a wave vector in the k_x k_y plane which was measured from the zone edge. The zero-order wave-function as those at the vertical edge

HKH of the Brillouin zone was used. The vectors of $k \cdot p$ expansion will converge rapidly due to the small dimensions of the Fermi surface in the k_x k_y directions. The minimum number of independent parameters was determined using symmetry. The effective mass Hamiltonian of the Slonczewski-Weiss-McClure band model is given as in figure 5. This was used by the authors to determine the electronic energy band parameters of graphite as in table 1 [2, 18]. The 7 parameters are defined as γ_0 which describes the electron hopping within each layer leading to linear dispersion near the neutrality point. γ_1 describes coupling between orbitals in atoms which are closest in successive layers. γ_3 and γ_4 describes hopping between orbitals of atoms which are closest in successive layers. The coupling between orbitals and its nearest neighbour layers are described by γ_2 and γ_5 respectively. The inequivalence between two sublattices in each graphene layer is described by the onsite energy Δ taking the presence of neighbouring layers into account. The parameters of these values are dependent on inter layer pressure related to the interatomic distance between graphene layers [19]. The values of these parameters are presented in table 1 and an illustration of the parameters is presented in figure 6.

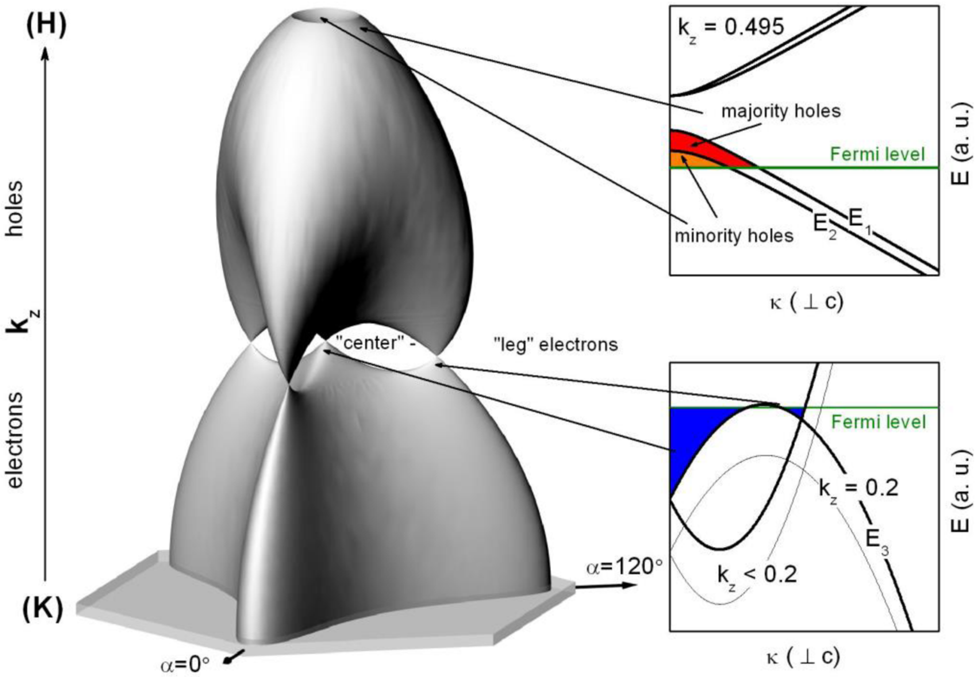

Figure 4: Fermi surface of graphite along the edge K-H with the electron pocket at the K point and the hole pocket at the H point calculated using Matlab. It has a trigonal symmetry, which is particularly distinct at the K point. The electron and hole pockets are connected by so-called "centre" and "leg" pieces, which originate from the overlap of the E3 bands (see lower inset). At the H point, an additional hole pocket, which is associated with the E2 band, is found (see upper inset). For illustration reasons the kz-values have been divided by a factor of 5[18].

$$H = \begin{pmatrix} E_1 & 0 & H_{13} & H_{13}^* \\ 0 & E_2 & H_{23} & -H_{23}^* \\ H_{13}^* & H_{23}^* & E_3 & H_{33} \\ H_{13} & -H_{23} & H_{33}^* & E_3 \end{pmatrix}$$

where

$$\begin{aligned} E_1 &= \Delta + \gamma_1\Gamma + \frac{1}{2}\gamma_5\Gamma^2, \\ E_2 &= \Delta - \gamma_1\Gamma + \frac{1}{2}\gamma_5\Gamma^2, \\ E_3 &= \frac{1}{2}\gamma_2\Gamma^2, \\ H_{13} &= -\gamma_o(1-\nu)\sigma \mathrm{e}^{i\alpha}/2^{1/2}, \\ H_{23} &= \gamma_o(1+\nu)\sigma \mathrm{e}^{i\alpha}/2^{1/2}, \\ H_{33} &= \gamma_3\Gamma\sigma \mathrm{e}^{i\alpha}, \\ \Gamma &= 2\cos(\pi\xi), \end{aligned}$$

and

$$\nu = \gamma_4\Gamma/\gamma_o.$$

Figure 5: Slonczewski-Weiss-McClure effective mass Hamiltonian model expression for graphite and calculation [2].

Table 1: Electronic energy band parameters of graphite [2].

Parameter	eV	Description of origin
γ_0	3.12	Overlap of neighbouring atoms in a single layer plane.
γ_1	0.377	Overlap of orbitals associated with A and A' atoms located one above the other in adjacent layer planes.
γ_2	-0.0206	Interactions between atoms in next nearest layers and from coupling between π and σ bands.
γ_3	0.29	Coupling of the two E_3 bands by a momentum matrix element.
γ_4	0.120	Coupling of E_3 bands to E_1 and E_2 bands by a momentum matrix element.
γ_5	0.025	Interactions between second nearest layer planes. Introduction in E_1 and E_2 in second order of Fourier expansion to be consistent with E_3.
Δ	-0.009	Potential energy differences at A and B lattice sites.

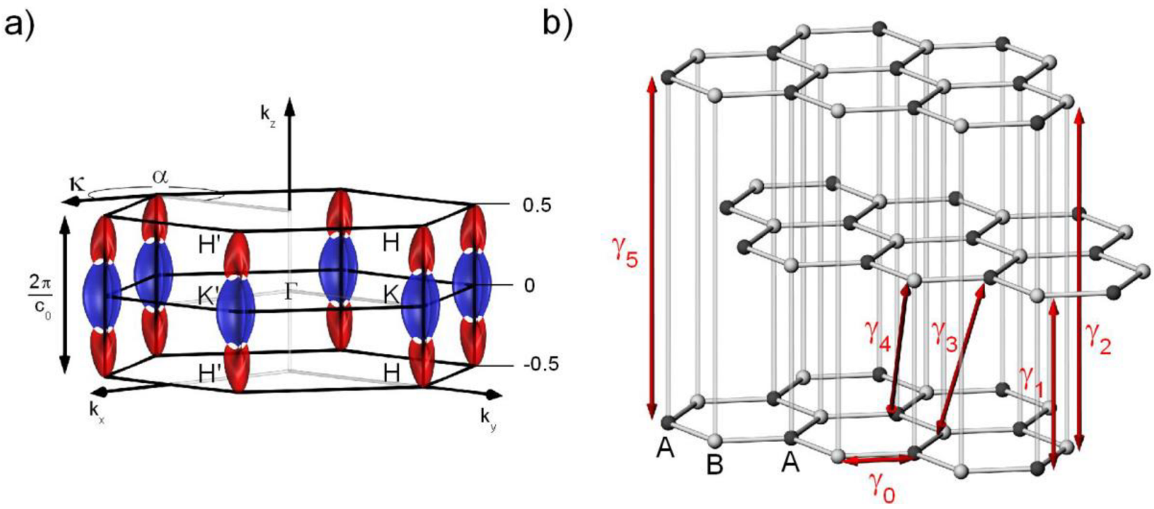

Figure 6: (a) illustration of the HKH zone (b) illustration of electronic energy band parameters in Bernal stacked graphite [18]

The energy dispersion relations are given by the eigen values of the Hamiltonian presented by the equation in figure 5. Two of the four solutions are doubly degenerate and correspond to E_3 along the zone edge HKH whereas two solutions are nondegenerate and correspond to E_1 and E_2 as in figure 3. At the H point where $\xi = 1/2$, E_1 and E_2 become degenerate. The double degeneracy of these levels and of the E_3 levels is maintained as one move away from the H point in the plane $\xi = 1/2$, as is shown in figure 3c [2, 18].

Electrical conductivity for graphite is difficult to measure along the intrinsic c-axis due to the layered nature of the substance. Table 2 indicates the theoretical conductivities for pyrolytic graphite as σ_a and σ_c, mobilities μ_a and μ_c, relaxation times τ_a and τ_c, mean free paths l_a and l_c and electron density n. The anisotropy ratio of σ_a/σ_c for pyrolytic graphite is $10^3 - 10^5$, however for single crystal graphite it is lower between 10^2-10^5 for reasons which are not well understood [2].

Table 2: Theoretical conductivities for pyrolytic graphite

Measurement	Units	300 K	77.5 K	4.2 K
σ_a	10^4 ohm^{-1}cm^{-1}	2.26	3.87	33.2
σ_c	Ohm^{-1}cm^{-1}	5.9	3.3	3.8
σ_a/σ_c	10^4	0.38	1.2	8.8
μ_a	10^4cm^2/V.s	1.24	5.75	7.0
μ_c	Cm^2/V.s	3.3	5.0	8.0
τ_a	10^{-13}s	3.5	16.2	196
τ_c	10^{-14}s	0.95	1.6	2.7
la	10^3Å	0.7	3.2	39
lc	Å	0.95	1.6	2.7
n	10^{18}cm^{-3}	11.3	4.2	3.0

2.3.Magnetic properties

The magnetic field is along the c-axis in the graphite structure. There are three constant energy orbits which are perpendicular to the HKH axis of the Brillouin zone corresponding to an extremum in the Fermi surface cross-sectional area at specific points along the HKH axis. The three constant energy orbit types are illustrated in figure 7 and their placement in figure 8. The first energy orbit in figure 7a corresponds to the extremal cross section on the majority electron surface at the K-point. The second orbit in figure 7b corresponds to extremal cross sections on the majority and minority hole surfaces at the H-point. The third orbit type in figure 7c corresponds to the external cross sections on the majority electron or majority hole surfaces at the points where these surfaces make contact known as leg and central orbits. The central leg orbit lies on the HKH axis and there are 3 other contact leg orbits where the surfaces make contact off the HKH axis [2].

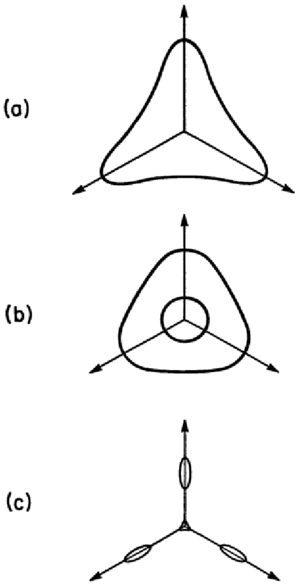

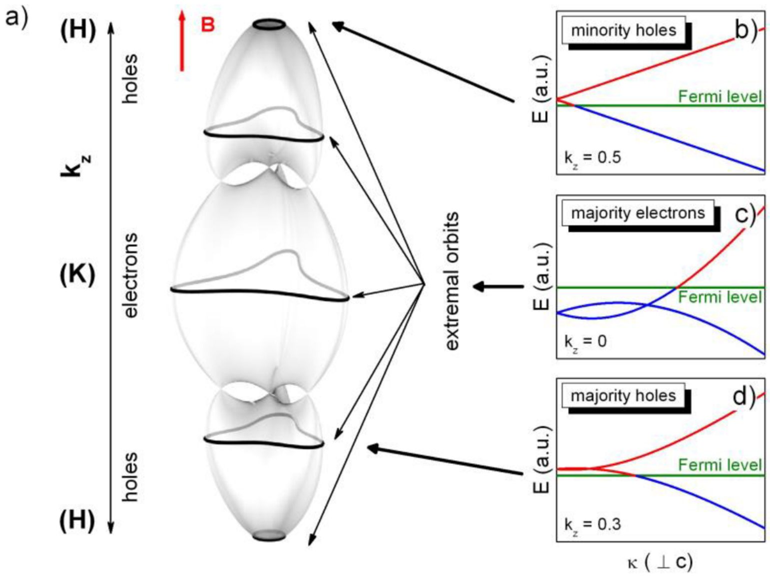

Figure 7 (left): Typical constant-energy orbits normal to the HKH axis. (a) Trigonally distorted orbit for majority electrons at the K point. (b) Cap orbits near the H point. The outer orbit is for the majority holes; the inner orbit is for the minority holes. (c) Leg and central orbits near the confluence of the electron and hole surfaces [2].

Figure 8(right): ***a)*** *Fermi surface of graphite along the edge H-K-H with its electron and hole pockets. For illustration reasons the value of kz has been devided by a factor of 2.5. The extremal orbits at the K point (kz = 0) and at kz _ 0:3 close to the H point (kz = 0:5) are due to majority electrons and holes, respectively. At the H point an additional extremal orbit, referred to as minority holes, is observed.* ***b)- d)*** *In-plane dispersion relation at kz = 0 (majority electrons), kz = _0:3 (majority holes) and kz = _0:5 (minority holes). While the in-plane dispersion relation is parabolic for the majority carriers, it is linear for the minority holes* [18].

2.4.Lattice properties

In graphite the E_{2g1} and E_{2g2} modes are Raman active and the E_{1u} and A_{2u} modes are infrared active while the silent modes are the B_{1g} and B_{1g2} modes as indicated in figure 9. The interlayer phase difference between the E_{1u} and E_{2g2} modes is a measure of the interlayer force constant of the graphite lattice indicated by the frequency difference. The E_{2g2} mode frequency of~ 1582 cm^{-1} observed in HOPG is close to the C-C vibrational frequency of 1584.8 cm^{-1} in the benzene molecule. The first order Raman frequency is ω_R =1581 cm^{-1} and the second order Raman line lies at 3248 cm^{-1} with a peak upshift of 86 cm^{-1} from $2\omega_R$. The E_{2g1} mode is estimated to be at~210 cm^{-1}, but this is still relatively unknown. A Raman line at 1355 cm^{-1} has been observed in commercial graphite which may be related to an sp^3 carbon structure with a vibrational frequency at 1322 cm^{-1} as observed in diamond [2].

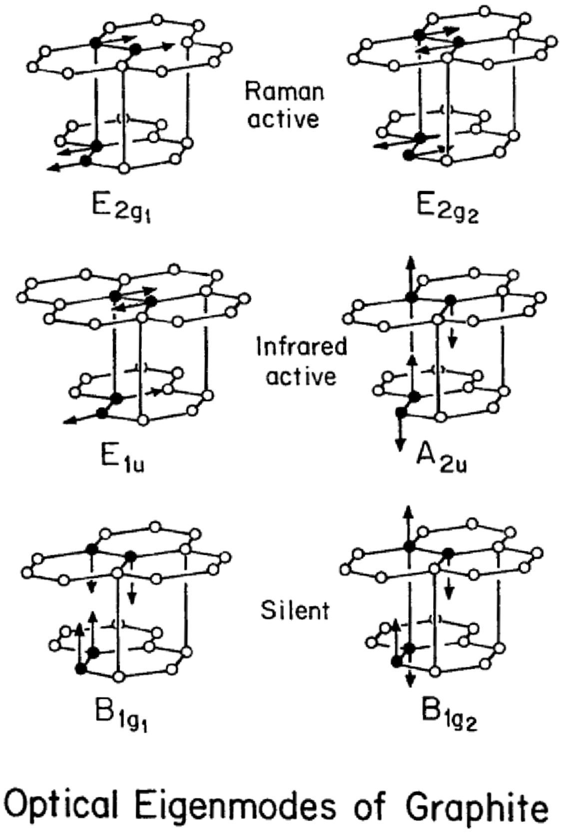

Figure 9: Optical lattice vibrational modes of graphite [2]

3. Surfactants for carbon nanoparticle dispersion

Surfactants are a diverse class of chemicals, and its very name is a contraction of the words "surface active agent". Therefore, it is a common tool to influence the surface energy of substances. Surfactants are used to maintain the stability of dispersed phases by surface interaction. Surfactants are amphiphilic since they are comprised of both hydrophilic and hydrophobic parts within each micelle [20]. The micelle for decyl glucoside is presented in figure 10. It is comprised of a hydrophilic "head" and a hydrophobic alkyl "tail". The hydrophilic tail part of the micelle interacts with the water to provide colloidal stability and avoiding particle agglomeration. The hydrophobic tail interacts with the hydrophobic carbon particle by adhering to the particle surface by physio adsorption [21, 22]. Surfactants are categorised in 4 groups namely non-ionic, anionic, cationic, and amphoteric. Decyl glucoside is a non-ionic surfactant with surface tension contained between 30 – 40 mN/m [23]. Decyl glucoside is a bio-surfactant meaning it is biologically derived. It is more environmentally friendly than surfactants derived from petrochemicals. Previous research suggested that non-ionic surfactants were better for maintaining carbon dispersions in aqueous media over a wide pH range [24, 25]. Non-ionic surfactants mechanisms of dispersion using carbon particles is mainly due to steric forces rather than electrostatic forces observed when using ionic surfactants [25].

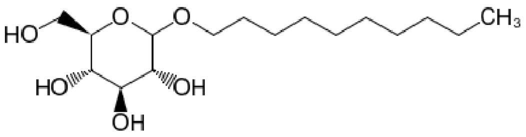

Figure 10: Chemical structure of decyl glucoside micelle

4. Measurement of electrical properties

Electrical resistance is directly related to electrical conductivity. Electrical resistance (Ohms) is defined by Ohms law as the potential applied to a sample (Volts) divided by the current (Ampere). Thus, electrical resistance of samples with varying conductive properties can be measured by influencing the applied potential or current. Electrical resistance describes the overall resistance to current flow of a sample depending on its dimensions and type of material. Electrical resistivity is defined as the resistance to electrical current flow of an object per unit length. The electrical resistance of planar structures is defined by their surface resistivity (ρs) and volume resistivity (ρv). The surface resistivity can be calculated from the measured surface resistance (Rs = Ω) according to equations 1 and 2 respectively. Volume resistivity can be calculated using the measured volume resistance (Rv = Ω.cm) and equations 3 or 4 [26].

Equation 1: Calculation of surface resistivity

$$\mathrm{\rho s} = \mathrm{Rs}\frac{D}{L}$$

Equation 2: Calculation of surface resistivity when electrode dimensions are known

$$\mathrm{\rho s} = \mathrm{Rs}\frac{o}{g}$$

Equation 3: Calculation of volume resistivity

$$\mathrm{\rho v} = \mathrm{Rv}\frac{A}{L}$$

Equation 4: Calculation of volume resistivity when electrode dimensions are known

$$\mathrm{\rho v} = \mathrm{Rv}\frac{A}{t}$$

For equation 1 the surface resistivity (Ω) is calculated using the surface resistance (Rs), distance between electrodes (L) and unit width (D). For equation 3 the volume resistivity (Ω.cm) is calculated using the volume resistance (Rv), distance between electrodes (L) and cross-sectional area of the sample surface underneath the electrodes (A). Typically, electrodes with known dimensions are used and therefore equations 2 and 4 apply to measure the surface and volume resistivity of samples respectively. For equation 2, o is defined as the effective perimeter of the electrode used and g is the distance between the guarded and ring electrodes. For equation 4, A refers to the effective area of the measuring probe and t is the sample thickness [26].

5. Reviewed literature

Chen et al. dispersed graphite nanosheets in a PMMA matrix. The authors used natural flake graphite which was treated with a 4:1 v/v ratio of sulfuric and nitric acid to produce expanded graphite. The reaction mixture was continuously stirred for 16 hours and neutralized with water before being dried. The treated graphite articles were then heat treated at 1050 °C for 15 seconds. The heat treatment resulted in an expansion of the graphite to 300 % the original dimensions in the c-direction [27]. A SEM image of the prepared expanded graphite is presented in figure 11. Graphene nanoplatelets can be produced by mechanical agitation of expanded graphite through solvent exfoliation by sheering or sonication. Sonication or sheering of expanded graphite can cause defects and a decrease in lateral layer size resulting in decreased electrical conductivity [28].

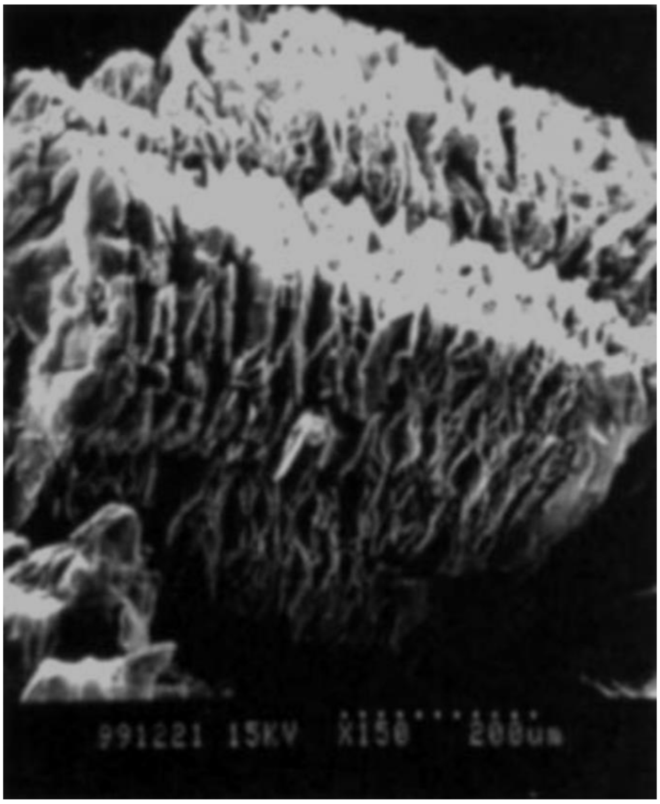

Figure 11: SEM of expanded graphite [27]

The authors placed a mixture of 1-10 % expanded graphite mixed with MMA in the presence of 0.5 wt% BPO in a sealed vessel. This was heated to 150 °C for 30 min. Upon cooling a black solid was formed. The solid was crushed and mixed with 1 part PVC resin and PMMA/graphite respectively, 0.8 DOP and 0.003 Tin mercaptide. The resulting mixture was rolled on a twin roller for 8 min and moulded [27]. Conductivity measurements of the prepared samples are illustrated in figure 12.

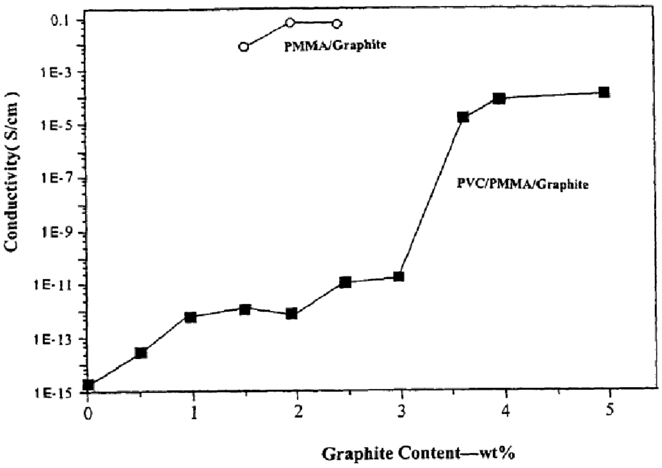

Figure 12: Volume conductivity vs graphite weight percentage of respective samples at room temperature [27]

It was noted that the volume conductivity for the samples increased as the weight percentage of graphite increased. For the PVC/PMMA/expanded graphite composite the percolation threshold was determined to be 3.5 % filler content, which was much lower compared to conventional conductive composites. The maximum conductivity of 10^{-4} S/cm was reached at 5.0 wt% expanded graphite. This was stated to be 40 % lower filler content to achieve the same conductivity using graphite powder with 20µm particle size. It was stated that the addition of PVC resin possibly contributed to the destruction of conductive networks within the composite resulting in reduced conductivity. This destructive effect was also observed when rolling was too intense. The addition of graphite to the composite also resulted in an increase in tensile strength with the 5 wt% graphite sample exhibiting a 30% increase in tensile strength compared to a sample with no filler [27].

Kausar. A, investigated carbon filler containing composites like which was produced by Chen et al. The author focussed on a PMMA matrix with graphene, graphene oxide and graphite as nanofillers. The composites with respective fillers at various ratios and fabrication techniques are presented in the table 3. Comparison of investigated results revealed that the electrical conductivity of the PMMA/graphene nanocomposites was very high at increased filler loading level. A sample containing 8 wt% expanded graphite exhibited one of the highest electrical conductivities of 60 S/m^{-1} with lower values obtained with lower filler content. The PMMA/RGO sample containing 2.7 vol% filler produced by latex technology exhibited the highest electrical conductivity of 64 S/cm^{-1}. This was very high compared to other RGO samples, and the difference could be attributed to the fabrication technique. Fabrication using the latex technique proved to produce better interaction between the filler and polymeric phase to form a network structure with superior conductive pathways. GO also possibly reduced segmental mobility within the PMMA polymer resulting in higher glass transition temperatures. Increased filler content also resulted in higher composite tensile strength. Other RGO samples exhibited very low electrical conductivity like the non-conductive GO samples. The GO samples exhibited no measurable electrical conductivity since GO is an electrical insulator in the absence of moisture [29, 30].

Table 3: Comparison of PMMA/graphene, GO, RGO and graphite fillers conductivity, tensile strength and glass transition temperatures [30]

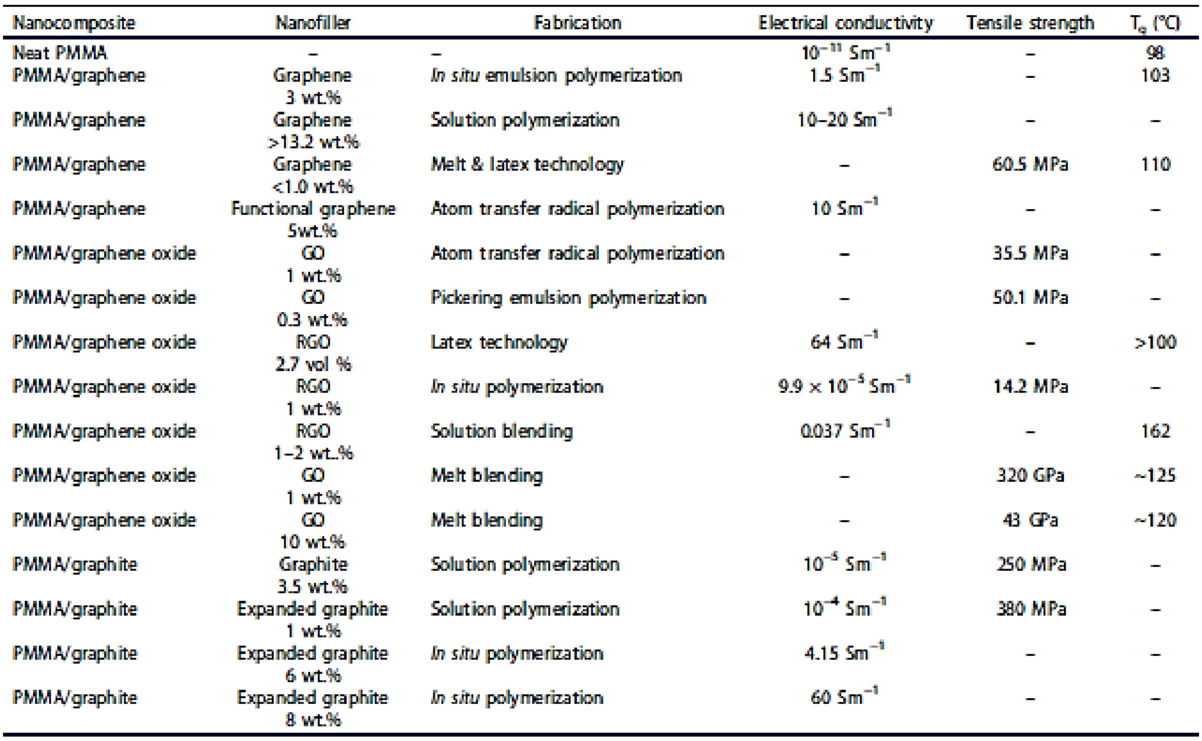

Nanocomposite	Nanofiller	Fabrication	Electrical conductivity	Tensile strength	T_g (°C)
Neat PMMA	–	–	10^{-11} Sm^{-1}	–	98
PMMA/graphene	Graphene 3 wt.%	*In situ* emulsion polymerization	1.5 Sm^{-1}	–	103
PMMA/graphene	Graphene >13.2 wt.%	Solution polymerization	10–20 Sm^{-1}	–	–
PMMA/graphene	Graphene <1.0 wt.%	Melt & latex technology	–	60.5 MPa	110
PMMA/graphene	Functional graphene 5wt.%	Atom transfer radical polymerization	10 Sm^{-1}	–	–
PMMA/graphene oxide	GO 1 wt.%	Atom transfer radical polymerization	–	35.5 MPa	–
PMMA/graphene oxide	GO 0.3 wt.%	Pickering emulsion polymerization	–	50.1 MPa	–
PMMA/graphene oxide	RGO 2.7 vol %	Latex technology	64 Sm^{-1}	–	>100
PMMA/graphene oxide	RGO 1 wt.%	*In situ* polymerization	9.9×10^{-5} Sm^{-1}	14.2 MPa	–
PMMA/graphene oxide	RGO 1–2 wt..%	Solution blending	0.037 Sm^{-1}	–	162
PMMA/graphene oxide	GO 1 wt.%	Melt blending	–	320 GPa	~125
PMMA/graphene oxide	GO 10 wt.%	Melt blending	–	43 GPa	~120
PMMA/graphite	Graphite 3.5 wt.%	Solution polymerization	10^{-5} Sm^{-1}	250 MPa	–
PMMA/graphite	Expanded graphite 1 wt.%	Solution polymerization	10^{-4} Sm^{-1}	380 MPa	–
PMMA/graphite	Expanded graphite 6 wt.%	*In situ* polymerization	4.15 Sm^{-1}	–	–
PMMA/graphite	Expanded graphite 8 wt.%	*In situ* polymerization	60 Sm^{-1}	–	–

Marinho et al. electrical conductivity differences between graphene, MWCNT, carbon black graphite powder in the form of compact materials and in paper films. The conductivities of both paper film and compact samples were studied as a function of sample bulk density ρ = m/Al, where m is the material mass. A is the surface area and thickness l. The materials were first degassed for 12 hours in a vacuum at 150°C. Paper film samples were prepared by first dispersing the filler materials in a mixture of 1 part polystyrene sodium sulfonate and 1-part distilled water. The dispersion process was assisted by sonication with the container submerged in an ice bath. 10ml of the prepared dispersion was filtered through a polyamide membrane with a 0.45 µm pore size and pressurized. A smooth black film formed on top of the filter because of sedimentation. This was dried for 3 hours at 90°C under a 200-

400 mbar vacuum. The DC electrical resistance of both paper film and compact type samples were measured 6 times with applied current and the resistance was calculated using Ohm's law. It was noted for each of the samples tested the bulk conductivity measured did not reach that of a single particle possibly due to the contact resistance effect. This effect was more prominent for the nanostructures MWCNT and graphene by up to 6 orders of magnitude compared to the microstructures. Previous studies have shown an increase in particle size had related to an decreasing effect of contact resistance which improved the electrical conductivity of a bulk composite [31, 32]. Powder compaction analysis revealed that the bulk conductivity depended mainly on the packing density. The conductive behaviour of anisometric graphite was attributed to 2 mechanisms of which in the first pressing stage the sample density is controlled by rearrangement and fragmentation of agglomerates, followed by a second stage where the density is determined by elastic and plastic deformation. For MWCNT and graphite the filler orientation of the proved to have a significant influence on the bulk conductivity behaviour. For these types of anisometric nanoparticles with high surface area the powder pressing conductivity curves showed unexpected low values due to the contact resistance effect. Paper film samples produced with these nanoscale materials differed less from the single particle conductivity compared to the compact powder samples. This was indicated by the MWCNT paper film sample reaching a maximum conductivity of around 5×10^3 S/m measured in the in-plane direction and 1.4×10^3 for graphite paper film sample. It was stated that the influence of the surfactant used on the conductivity measurements was negligible [33].

Song et al. developed conductive composite films using graphite for use as antennas. The authors designed and prepared a flexible graphite film with an electrical conductivity as high as ~10^6 S/m by carbonizing and graphitizing a polyimide polymer film. Firstly, a polyimide membrane was slowly heated to 1300 °C in a continuously vacuumed electric furnace for 5-8 hours to promote carbonization. This was used to form an amorphous carbon structure and decompose non-carbon atoms. This was followed by firing the carbonized structure at 2850°C in and argon atmosphere to further improve the electrical conductivity. This is achieved since a complete sp^2 graphitic structure is formed under these conditions. Finally, to achieve a highly oriented and densely packed flexible graphene film structure the formed graphitic structure was subjected to a rolling process. There is a difference in the graphitic structure when producing graphite from polymers such as polyimide. This is due to the random overlaps of polyimide film resulting in turbostratic stacking of graphite layers in the final structure. The authors used the four-probe detection method to verify the electrical conductivity of the produced material which was 1.1×10^6 S/m and a surface resistance of 2.5×10^2 Ω/sq. this result was very close to the electrical conductivity of copper which is 1.3×10^7 S/m. The carrier concentration of the flexible graphene film was determined to be 808.8 $cm^2/V.sec$ which would make the material good for use as a performance antenna. The graphene film structure was about 5 times lighter compared to copper which is conventionally used for the same purpose [34].

Nagata et al. investigated the effects of graphite particle size on the electrical conductivity in LDPE/graphite composites. Graphite particles with dimensions indicated in table 4 were dried at 150°C for 24 h under vacuum. The authors dissolved LDPE in cyclohexane at 85 °C and mixed the graphite particles in a volume fraction range of 0 to 0.6 using a rotary evaporator. The cyclohexane was evaporated under vacuum conditions at 85°C. Subsequently, the materials were mixed in a hot roll for 10 min at 120°C. The resulting materials were pressed at 160°C under a pressure of 184 kg/cm^2 into sheets of 1- or 2-mm thickness. This was followed by quenching the composites at 15°C. A three-probe method was used to determine the electrical conductivity, σ, of the samples with and electrometer when the electrical conductivity was less than 10^{-10} S/cm or a two-probe method with a direct current power supply above this threshold [35]. Results of the measured conductivity are illustrated in the graph of figure 13.

Table 4: Physical properties of graphite particles [35]

Sample	Particle size (μm)	Specific surface area (m^2/g)
SGP-1	2.1	21.1
SGP-5	5.8	13.2
SGP-15	14.5	8.7
SGP-25	25.7	5.9
SGP-50	50.8	3.6
SGP-80	82.6	1.9
SGP-6 (spherical particle)	5.1	2.4

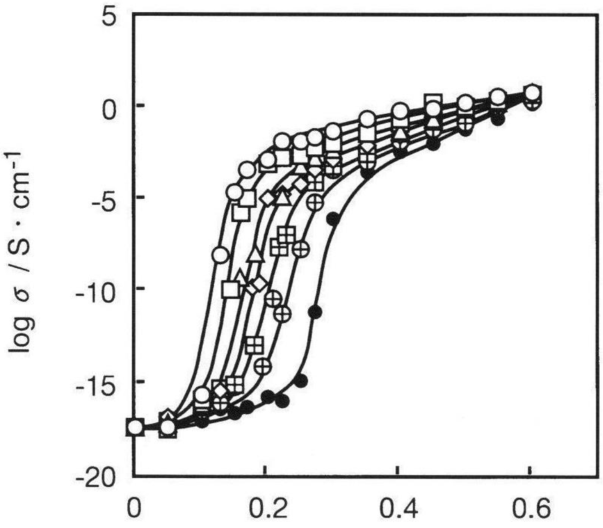

Figure 13: Electrical conductivity of samples with respect to volume fraction [35]

It was noted that the percolation theory was evident in the results since the materials went from being an electrical insulator to an electrical conductor over a very short range of filler content as indicated by the critical volume fraction, Φ_c, in table 5. It was determined that with an increase in particle size the critical volume fraction increased correspondingly. The critical volume fraction was higher for spherical particles compared to the plate like particles. It was found through crystallography that the orientation of the plater like particles were mostly in plane due to the rolling method applied which contributed to effective conductive pathway formation in the composites compared to the distributed spherical particles. The finer particles were also able to form more conductive pathways in the LDPE polymer resulting in a lower critical volume fraction and higher electrical conductivity [35].

Table 5: Critical volume fraction of samples compared to particle size [35]

Mean particle size (μm)	Particle critical volume fraction Φ_c
2.1	0.135
5.8	0.140
14.5	0.168
25.7	0.178
50.8	0.235
82.6	0.255
5.1(spherical particle)	0.292

Liu et al. produced composites containing graphite flakes and copper powder to investigate the interaction between the two substances on the overall composite properties. Graphite and copper are non-reactive and immiscible. The authors produced a powder where the graphite flakes were coated with copper by a copper plating process. the graphite flakes were fist cleaned and dried followed by activation with a solution containing $AgNO_3$ and NH_3. This was followed by a reduction with NaH_2PO_2 and rinsed with water each time after repeated reductions. Copper plating occurred by placing the treated graphite in a coating bath with $CuSO_4.5H_2O$, HCHO (37%), $Na_2EDTA.2H_2O$, $C_4H_4KNaO_6.4H_2O$ and bipyridine, at 45 °C and pH 12 which was adjusted using NaOH. The formed powder was washed to a neutral pH and dried under vacuum. The particles were then reduced under a hydrogen atmosphere for 2 hours at 400 °C. To form the composite the powder particles were mechanically mixed by V-mixer milling for 20 hours and loaded in a cylindrical graphite die. The furnace was heated to 1030°C at a rate of 10 °C/min and was held for 30min under a vacuum atmosphere. Once the temperature was over 600°C a pressure of 37 MPa was applied. The formed composite was then cooled to room temperature in the furnace [36].

It was determined that for the same volume fraction of graphite particles the electrical conductivity increased with increase in particle size. This related to a lower percolation threshold observed for larger particle sizes as illustrated in table 6. As a composite the electrical conductivity was lower than that of pure copper as seen by the low percentage against the IACS with 100% being excellent. This was attributed to the difference in conductive mechanisms since graphite conducts electricity with π-electrons compared to the free electrons in metals such as copper. The thermal conductivity was found to increase with an increase in graphite particle size due to the higher thermal conductivity of graphite compared to copper [37]. The tensile strength of the composites decreased with increase in particle size due to a decrease in grain boundaries within the composite [8, 36].

Table 6: Electrical conductivity of samples relative to graphite flake particle size compared to copper [36]

Particle size (µm)	Volume fraction (%)	IACS (%)
292	72.08	14.71
121	72.08	14.07
99	72.08	11.69
86	72.08	6.83
62	72.08	5.84

6. Experimental setup

6.1.Materials

The carbon filler materials used in the developed coating was graphene powder (20-30 µm, MST Latvia) and spherical graphite powder (1-3 µm, Epinikon a.s.). Highly branched PEI, Mw= 750 000 g.mol^{-1} (Lupasol® P, BASF), was used as crosslinking agent with Epoxy 200 V55, 455-525 g.mol^{-1} (Spolek pro chemickou a hutni vyrobu, a.s., Usti Nad Labem). Decyl glucoside non-ionic surfactant was used in samples which contained surfactant. The coating was applied onto a nonwoven viscose textile material (33.5 ± 3.3 g.m^{-2}) which was cut to samples sizes of approximately 15 cm x 15 cm. Methyl ethyl ketone (99%, Merck) was used in the MEK test for crosslinking strength.

6.2.Sample preparation

0.8 grams of polyethyleneimine was diluted with 2.5 grams of distilled water and stirred. The solution was added to respective amounts of carbon fillers as indicated in table 7 followed by ultrasonication (Bandelin Sonoplus LS 20) mixing for 5 minutes. Halfway through the mixing step, the samples were cooled to room temperature as well as after ultrasonication. The mixed solution of carbon fillers with PEI/H_2O was then added to 5.0 grams of Epoxy 200 V55 with stirring. The nonwoven textile material was immersed into the coating solution. Excess liquid was removed from the sample by vacuum. The samples were dried under vacuum for 24 hours followed by drying in the oven at 120°C for 1 hour. This process is illustrated as sample preparation method 1 in figure 14.

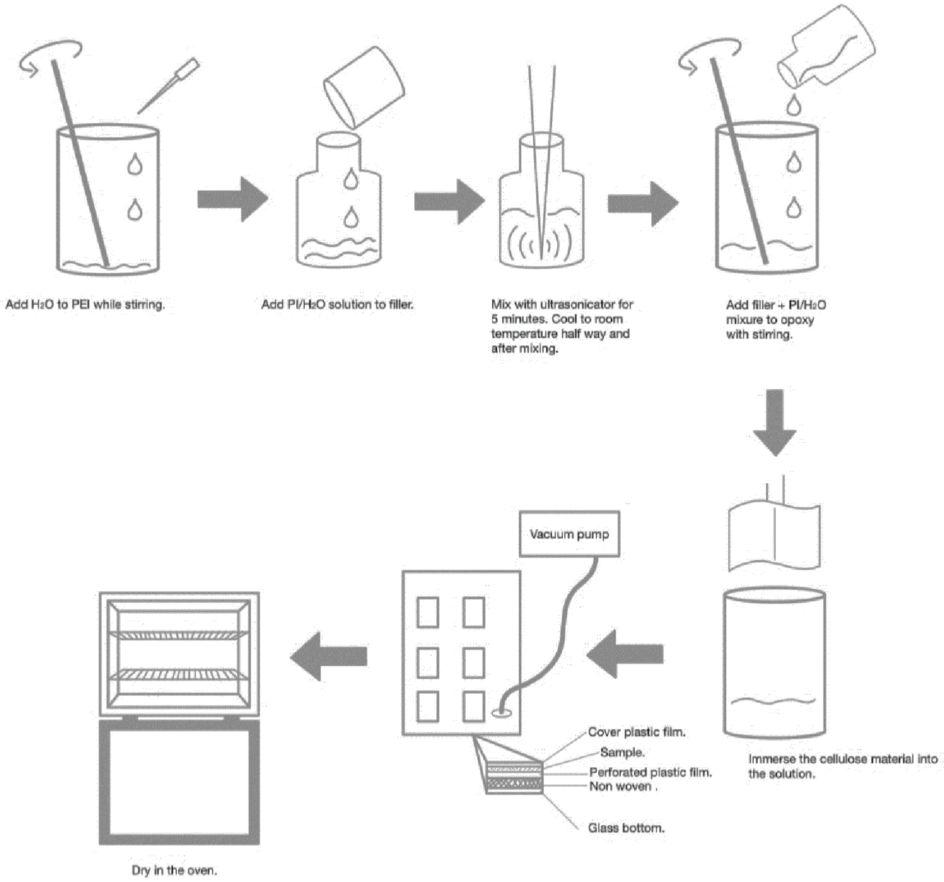

Figure 14: Sample preparation method 1

For samples prepared using sample preparation method 2, illustrated in figure 15, the same amount of PEI and distilled water was used with the respective amounts of carbon filler as indicated in table 7. This method omitted ultrasonication and samples were mixed by hand-stirring for 2 minutes before adding Epoxy 200 V55 followed by further stirring for 1 minute. Due to the increased viscosity the samples were padded with a solid hand roller and cured at 120 °C for 1 hour.

To promote filler mixing, 2.5 g 0.1% decyl glucoside/distilled water was added to samples 6, 11, 13 and 14 before mixing with PEI.

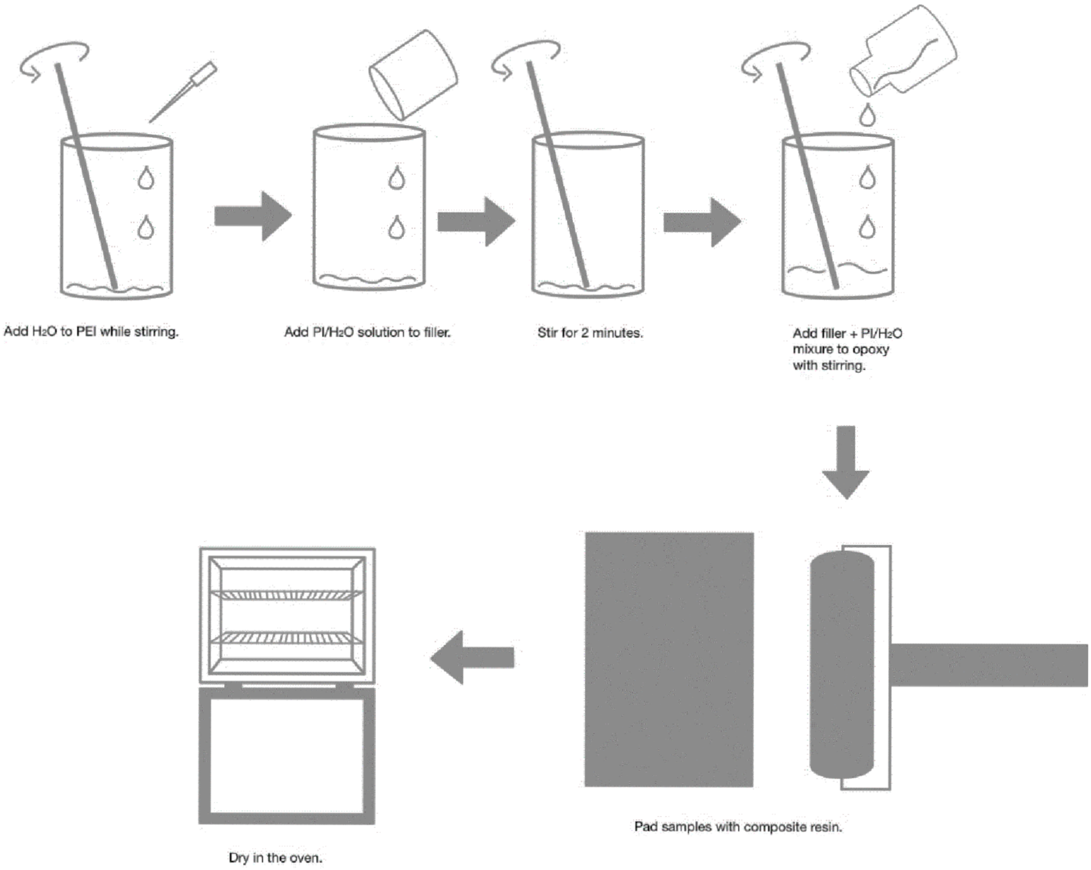

Figure 15: Sample preparation method 2

Table 7: Sample description

	Sample	Modification type	Surfactant use	Sample thickness (mm)	Sample weight after coating (g)	Sample weight after coating (g/m^2)	Sample weight increase by coating (%)	Amount of carbon in added coating (g)	Amount of carbon added in coating (g/m^2)
Preparation method 1	0	untreated	No	0.214	x	33.54	x	x	x
	1	M 0 % carbon filler	No	0.156	1.211	86.31	265.02	0.0000	0.0000
	2	M 1 % graphene	No	0.360	2.843	159.61	470.96	0.0284	1.2604
	3	M 2 % graphene	No	0.322	2.554	145.92	454.87	0.0511	2.2846
	4	M 3 % graphene	No	0.392	2.852	160.37	454.09	0.0856	3.7605
	5	M 5 % graphene	No	0.414	2.474	141.09	429.89	0.1237	5.4243
	6	M 5 % spherical graphite	Yes	0.172	0.702	64.17	192.49	0.0351	1.5448
	7	M 7 % graphene	No	0.356	2.711	154.83	457.67	0.1898	8.4872
	8	M 10 % graphene	No	0.332	2.315	134.53	410.47	0.2315	10.2088
Preparation method 2	9	M 20 % graphene	No	0.318	2.149	111.15	352.54	0.4299	15.9489
	10	M 40 % graphene	No	0.320	1.822	100.06	307.18	0.7287	27.0355
	11	M 40 % graphene	Yes	0.332	1.803	100.32	300.40	0.7212	26.8065
	12	M 60 % graphene	No	0.358	1.455	90.17	253.36	0.8729	32.7932
	13	M 60 % graphene	Yes	0.356	1.410	86.12	256.78	0.8461	31.5855
	14	Double layer M 60 % graphene	Yes	0.458	2.634	134.19	380.51	1.5802	59.4786

x = no coating

M = Epoxy + PEI

Measurement conditions: 52 % RH, 25.4 °C

6.3. Characterisation and testing methods

6.3.1. Material characterisation

Differential scanning calorimetry (DSC) was used to characterise the textile material as well as the coating to identify any physiochemical changes. The samples were subjected to heating at a rate of 10 °C/min from 25 °C – 300 °C in a nitrogen atmosphere. Microscopic analysis was performed by both optical- and scanning electron microscopy (SEM) on select coated samples. Optical microscopy images were made using a transmission scanning optical microscope with CCD Colour camera (Sony DFW-X710DK with Fibre finder Macro Video Navitar). A Vega 3 Tescan scanning electron microscope was used for SEM analysis. For fibre identification a Jenapol polarized light optical microscope (POM) in transmission scanning mode was used. This was coupled to an Imaging Source DFK 33UX25025710394 camera. The fibres were deposited on a glass slide in a drop of glycerine.

6.3.2. Crosslink strength (MEK) test

The solvent rub test was performed according to the ASTM D4752 standard to determine which curing temperature produced the most stable samples. This was done by subjecting samples cured at 40 °C, 80 °C, 100 °C, 120 °C to rubbing with methyl ethyl ketone expecting no physical changes after 200 rubbing cycles [38].

6.3.3. Measurement of electrical properties

The electrical resistance of the carbon fillers used was measured using an Agilent 53131A Universal counter at 1.00 V and 10 mA current. The electrode used is pictured in figure 16 with 1.00 kg of weight applied for compression of the powder. Measurements were made at 50 % relative humidity and 25.3 °C ambient conditions. The volume resistivity of each powder sample was then calculated according to equation 4. The surface and volume electrical resistivity of the textile samples were measured according to the EN61340-5-1:2001 standard for protection of electronic devices from electrostatic phenomena. Measurements were taken at 1.00 V and 10 mA. Ambient conditions during measurements were 42 % relative humidity and 23.8 °C. The electrical properties of the samples were measured using a Hewlett Packard 4339B resistance meter coupled to a ring electrode with dimensions according to the measurement standard. Sample dimensions were entered into the instrument and the resistivity was automatically calculated according to equations 2 and 4 for each sample.

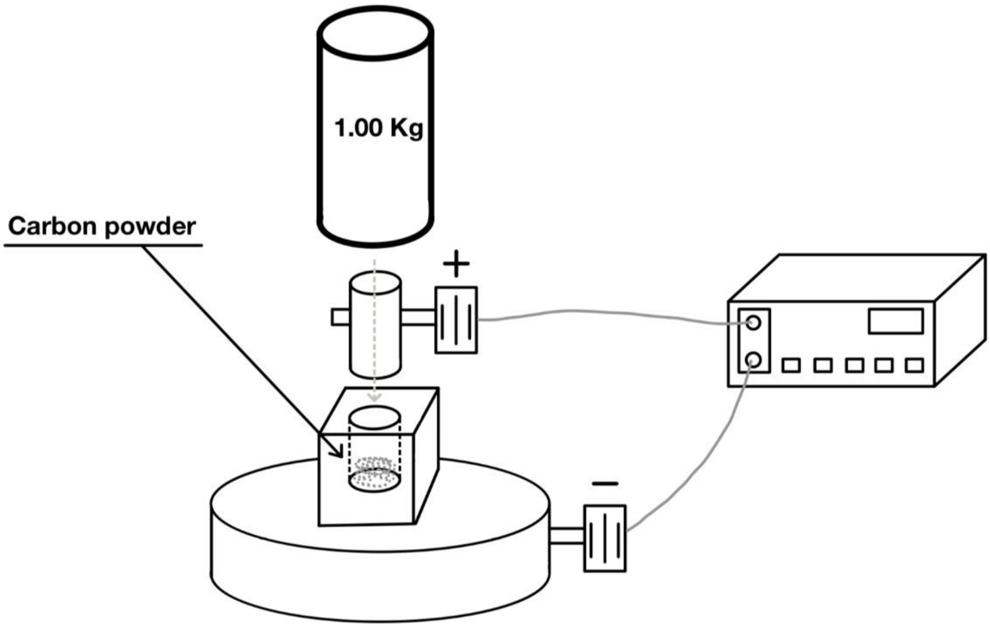

Figure 16: Electrode used in compact powder conductivity measurement

6.3.4. Measurement of EMI shielding effectiveness

EMI shielding was measured using a plane wave, far field EM wave over a frequency range of 30 MHz – 3 GHz according to the ASTM D 4935-99 standard for planar materials. The sample was held by a (Electro-Metrics, Inc., model EM-2107A) test fixture with dimensions according to the measurement standard. This was connected to an Agilent E5061B network analyser which was used to generate and receive the EM signals [39].

7. Results and discussion

7.1. Sample preparation observations

Sample preparation method 1 was first used to produce the textile materials. This method reached a limitation at 10 % filler content since it was not possible to continue with ultrasonication due to the viscosity increase and size restriction of the mixing vessel. Particle mixing become more problematic as viscosity increased due to the conversion of mechanical energy to heat. This heat can cause changes in the physical properties of the coating components as well as promoting the onset of curing [8]. It was therefore determined that hand mixing and a coating application by roller padding would be better suited as illustrated in sample preparation method 2. From table 7 it was determined that sample preparation method 2 resulted in less weight applied to the textile material on average compared to sample preparation method 1. Only 1 sample was prepared using the spherical graphite since even with the addition surfactant it still had difficulty mixing with the Epoxy/PEI coating system. This was the reason for the coating being unevenly distributed on the textile which also reduced the weight added to the textile material by the coating. Sample preparation method 2 was also determined to be the most practical sine it can be easily scaled. The differences in applied weight of the coating to the textiles was because of the variables in the coating application methods such as applied pressure to the roller. For sample preparation method 2 this could be improved by proper particle mixing as well as the use of a padder of which the applied pressure can be controlled. The sample thickness was directly related to the amount of weight added by the coating to the textile material. This was as expected since the sample surface area remained the same after coating.

7.2.Chemical process of crosslinking

Both Epoxy 200 V55 (0.1 – 0.7 Pa.s, 25°C) and PEI (25000 Pa.s, 20°C), with viscosities as indicated in the brackets, are miscible in water. For this reason, these materials were chosen as the polymeric constituents for the coating since the viscosity of the coating solution could be easily lowered by the addition of water. A chemical structure for highly branched PEI is illustrated in figure 17. Crosslinks are formed between the epoxy and PEI by nucleophilic addition reaction. This occurs when the ester groups in the epoxy reacts first with the active hydrogen of the primary amine in the PEI (Figure 18 a). This reaction can start to occur at room temperature. The product of this reaction is a secondary amine which can react further to form other secondary and/or tertiary amines respectively as illustrated in figure 18 b [10, 11].

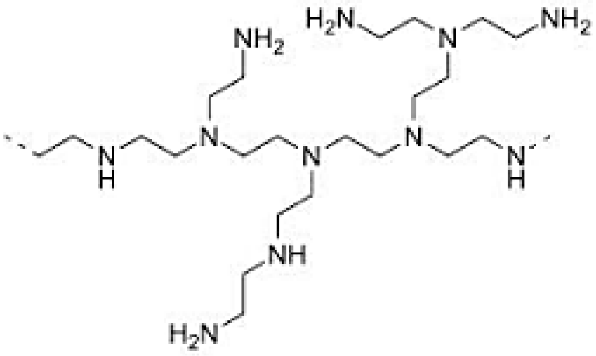

Figure 17: Structure of highly branched PEI [11]

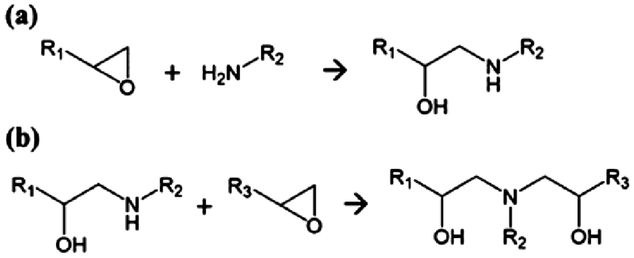

Figure 18: Reaction mechanism between epoxy and primary amine (a) and secondary amine (b) [10]

7.3. Differential Scanning Calorimetry (DSC)

A DSC graph of the nonwoven material is presented in figure 19. It is observed from the graph that there are no polymeric elements present in the material since there is no observable glass transition or melting of sample. The large endothermic curve with a peak at around 80 °C corresponds to the evaporation of water from the sample. There is however the onset of degradation at 236.60 °C. This DSC corresponds well with the identification of viscose as supported by the optical polarized microscopy image in figure 25 (right).

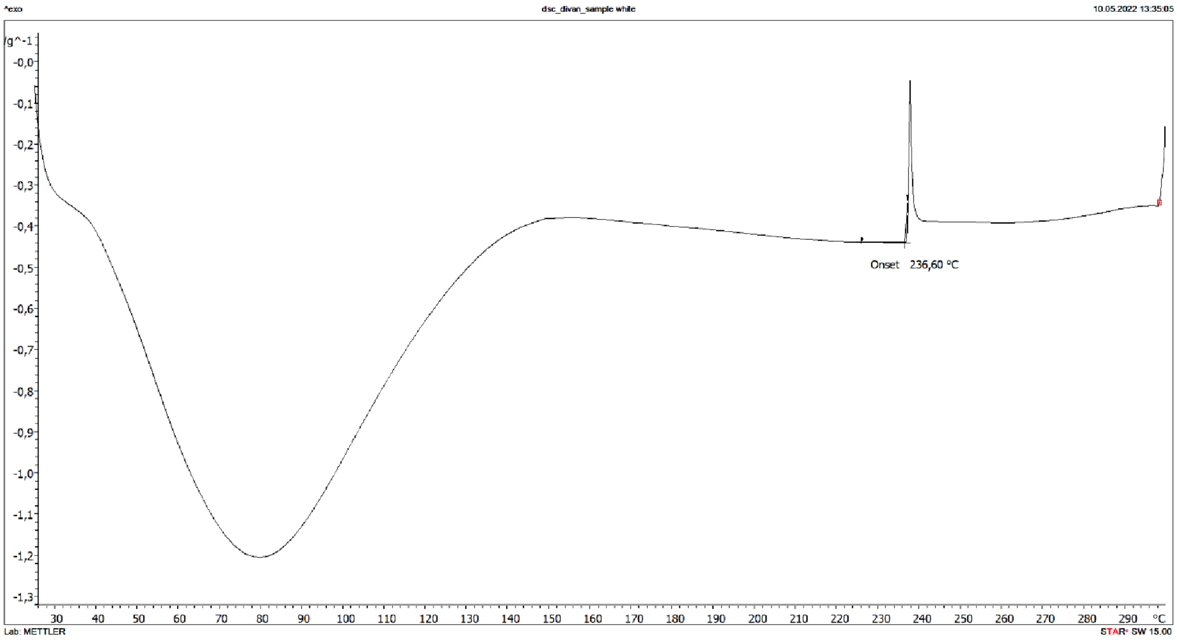

Figure 19: DSC of nonwoven textile material

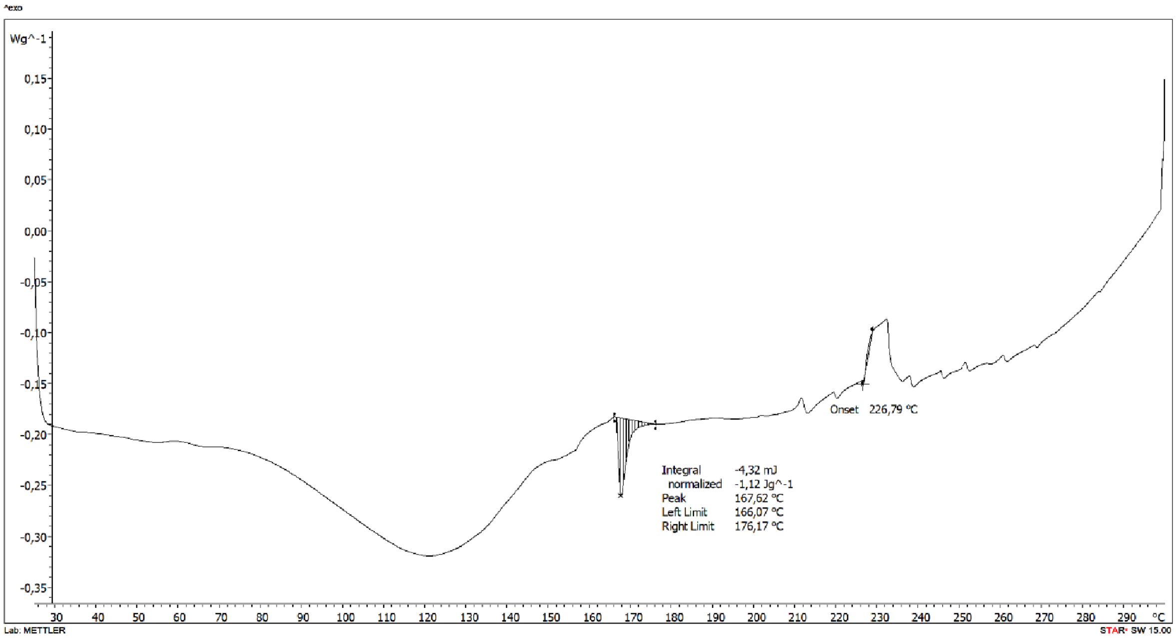

Figure 20: DSC of sample 1 with 0 % carbon coating

The textile sample containing 0 % carbon filler in the coating exhibited no distinguishable glass transition occurring as this was possibly hidden by water evaporation. It is suspected to be a small deviation from the base line at around 57 °C as supported by literature [11, 40]. The onset of degradation occurs at 226.79 °C which is as expected for viscose. At a peak of 167.62 °C there is an observable endothermic reaction. Since the applied coating is a thermoset polymer, it is not expected that this reaction is due to melting. It is suspected that water which was released during the earlier evaporation process facilitated the degradation of the coating which would start at the fibre-coating interface.

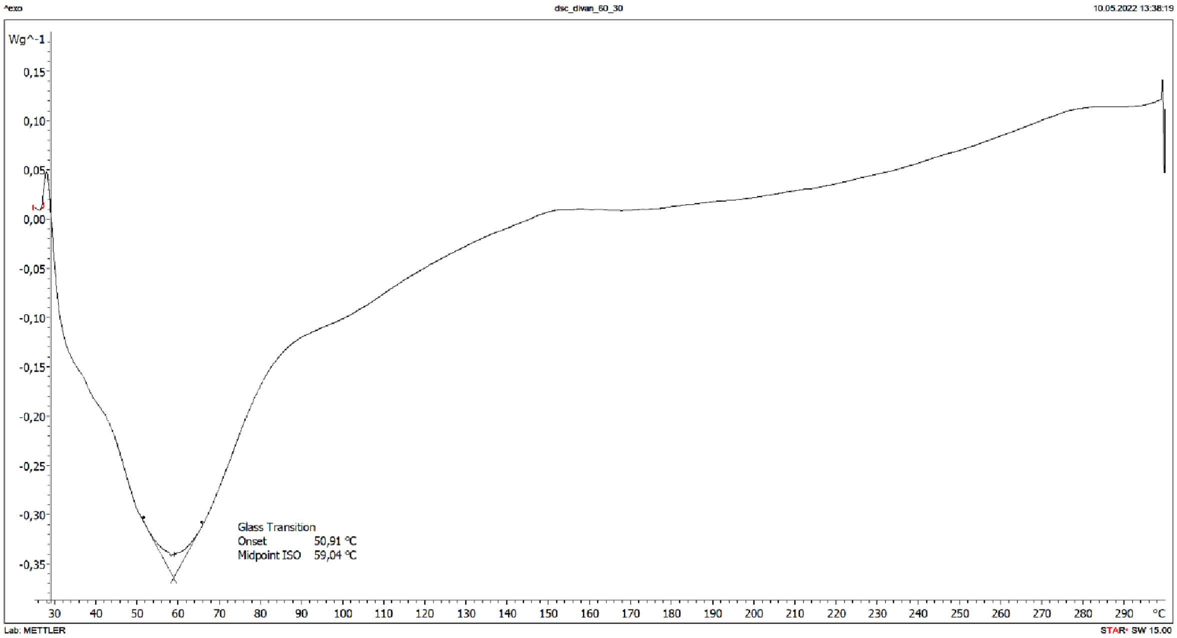

Figure 21: DSC of Epoxy/PEI/60%graphene coating (no textile)

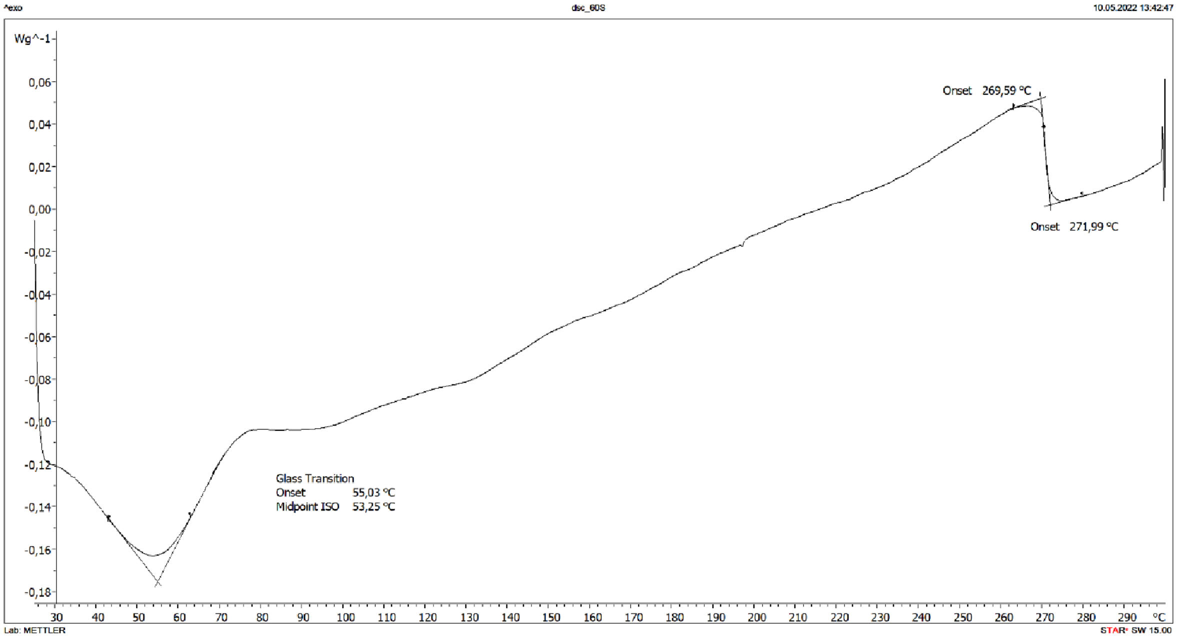

Figure 22: DSC of Epoxy/PEI/60% spherical graphite coating (no textile)

Figures 21 and 22 illustrates the DSC of coating materials containing the graphene and spherical graphite fillers respectively. Both graphs exhibit similar glass transition temperatures as expected for the Epoxy/PEI system of 59.04 °C and 53.25 °C respectively as stated in literature [11, 40]. Figure 22 depicts the onset of sample degradation at 271.99 °C, however this is not observable in figure 21. This could be due to the larger total surface area of the finer spherical graphite particle system compared to that of the larger graphene filler. This interface boundary is a relatively unknown part of any composite as this area possesses known individual characteristics of both matrix and filler elements as well as new synergistic characteristics. It is suggested that this is the reason for crosslink chain movement/degradation at this point. Due to the smaller total interface area of the larger particles this process is not so observable or could occur at a higher temperature.

7.4.Microscopic analysis

Scanning electron microscopy (SEM) images for the graphene and spherical graphite fillers are illustrated in figures 23 and 24 respectively. Figure 24 depicting the spherical graphite illustrates the layered structure of the graphite very well as expected. The particles exhibit visually accurate particle sizes as stated by the manufacturer to be 2 – 3 µm. Graphene is defined as a single layer of carbon, and it is therefore not expected to see the multi-layered structures observed in figure 23. The particle surfaces do appear as flat graphene sheets, however it was determined due to the layered structure of the particles the electrical properties will be anisotropic like that of graphite. From the image the particle size corresponds to the 20 – 30 µm stated by the manufacturer.

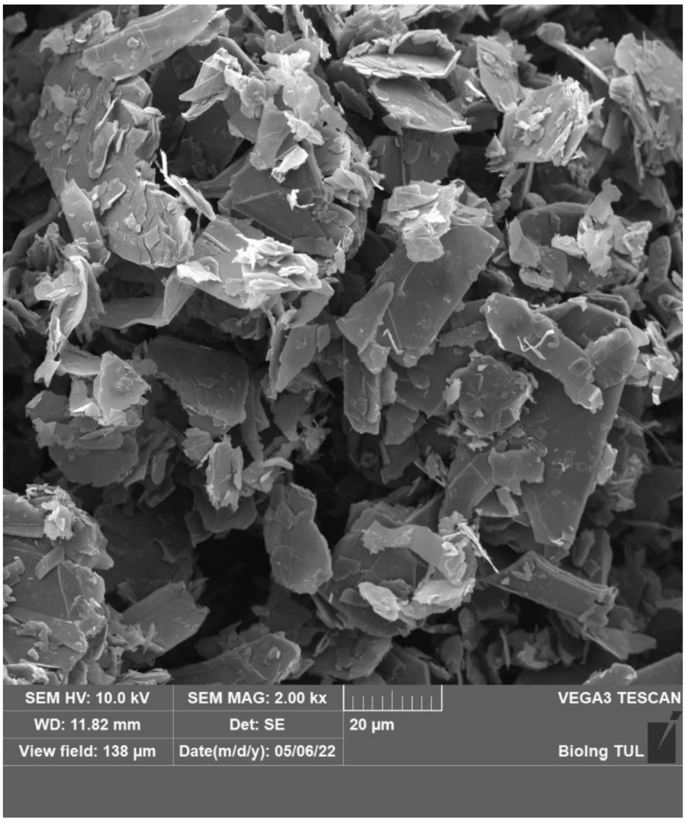

Figure 23: SEM of graphene particles

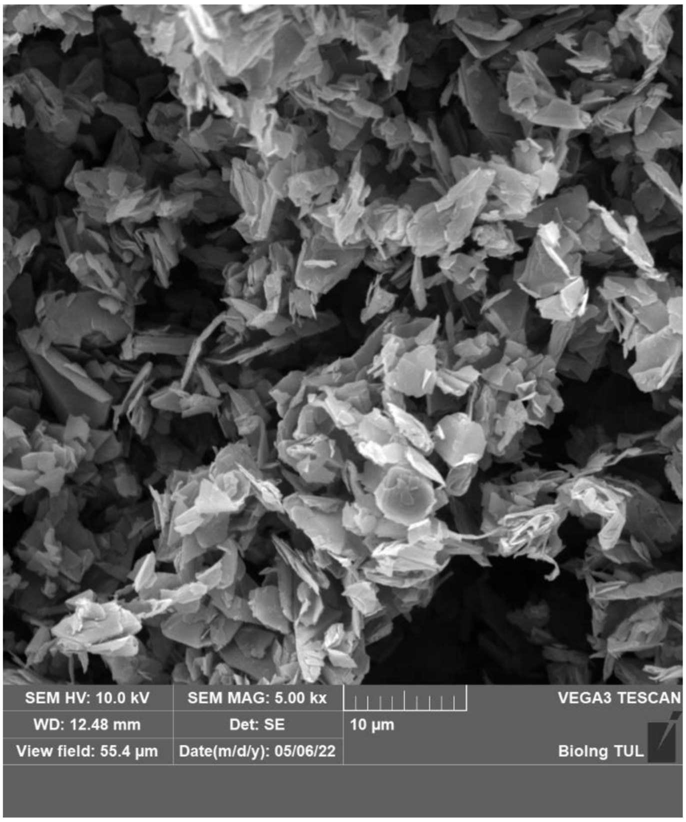

Figure 24: SEM of spherical graphite particles

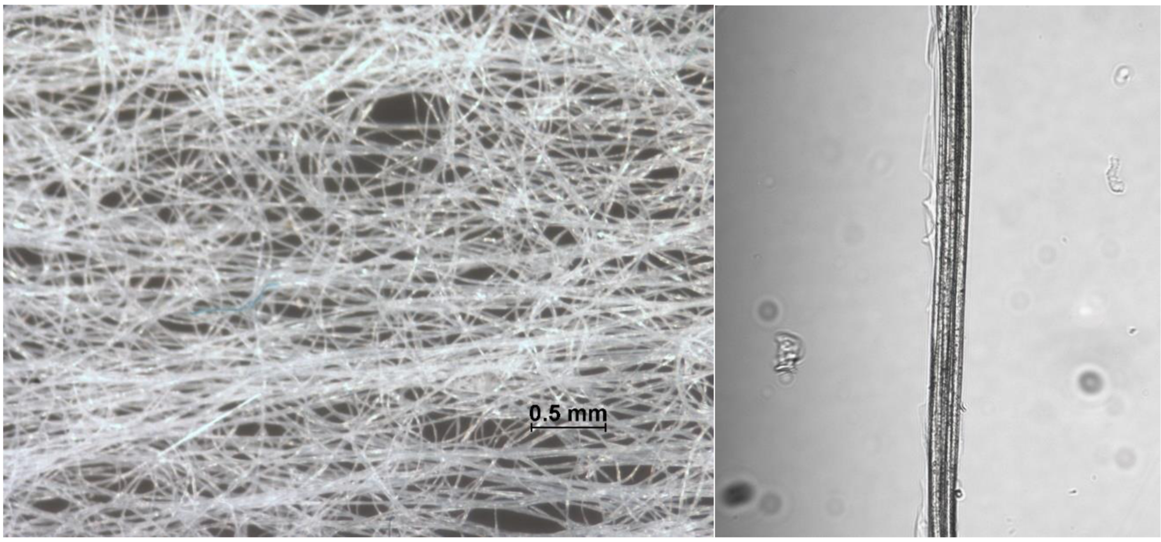

Figure 25: Untreated textile (Left) Optical microscope image (Right) POM image illustrating viscose fibre

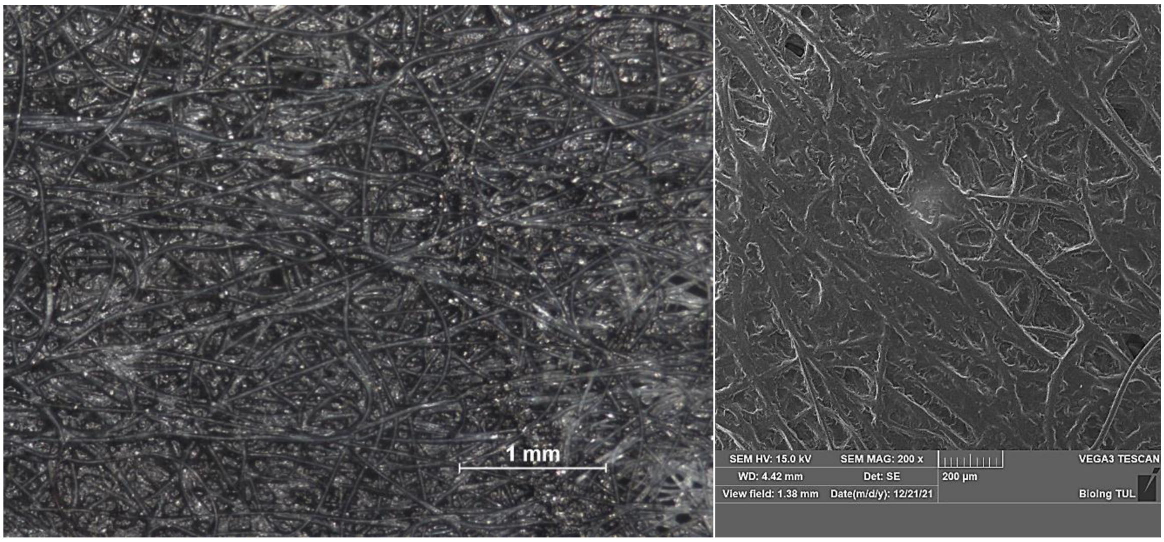

Figure 26: Sample 2 (Left) Optical microscope image (Right) SEM image

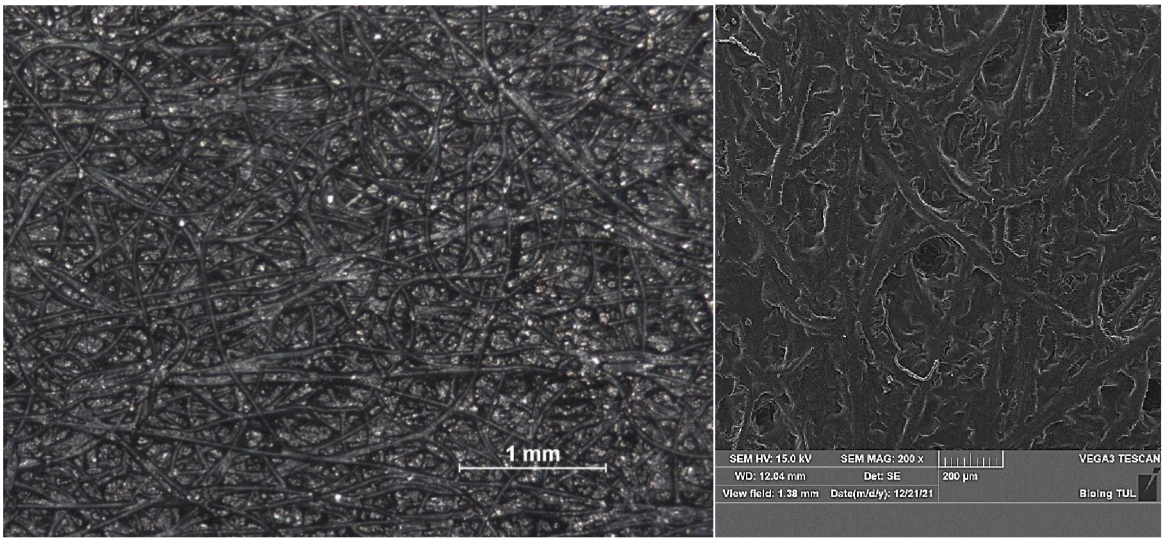

Figure 27: Sample 3 (Left) Optical microscope image (Right) SEM image

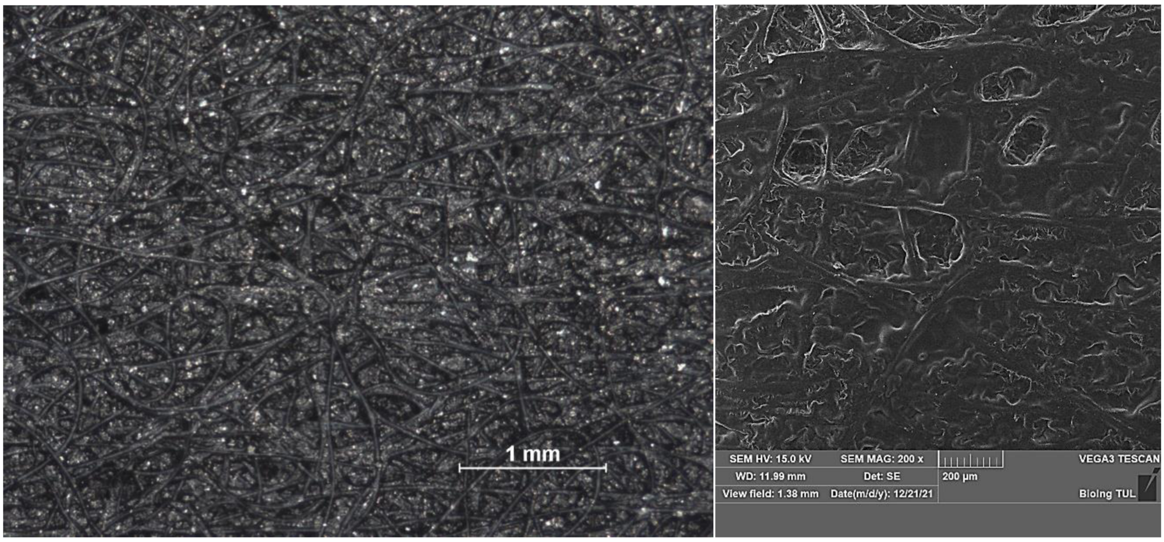

Figure 28: Sample 4 (Left) Optical microscope image (Right) SEM image

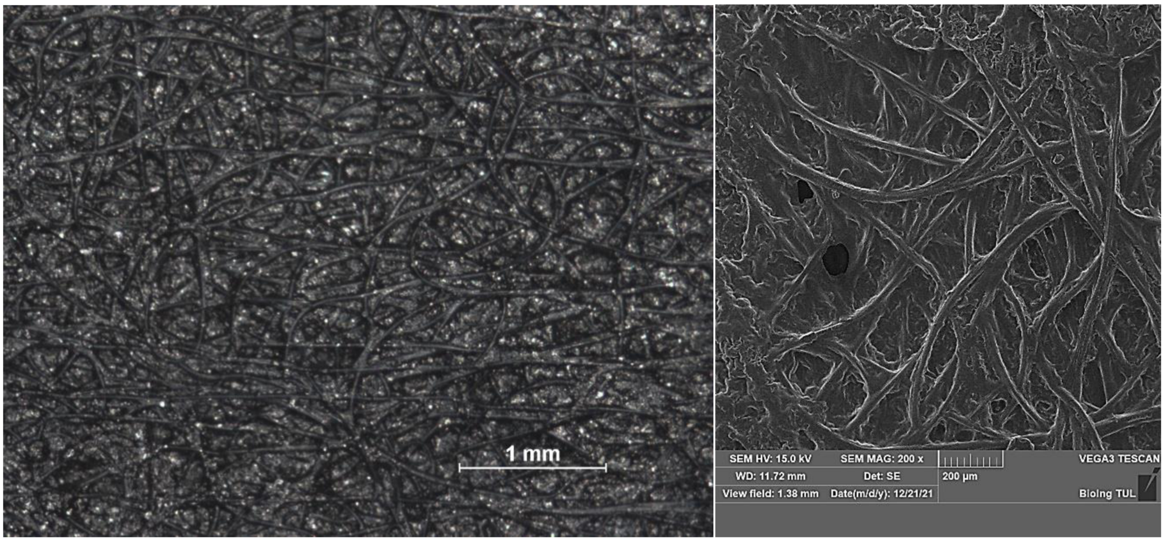

Figure 29: Sample 5 (Left) Optical microscope image (Right) SEM image

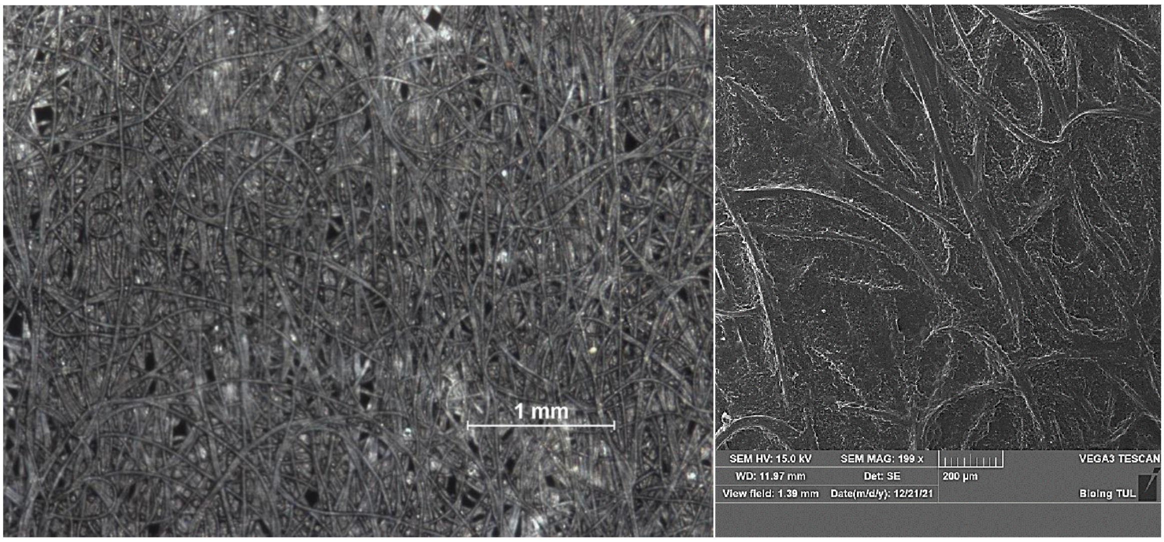

Figure 30: Sample 6 (Left) Optical microscope image (Right) SEM image

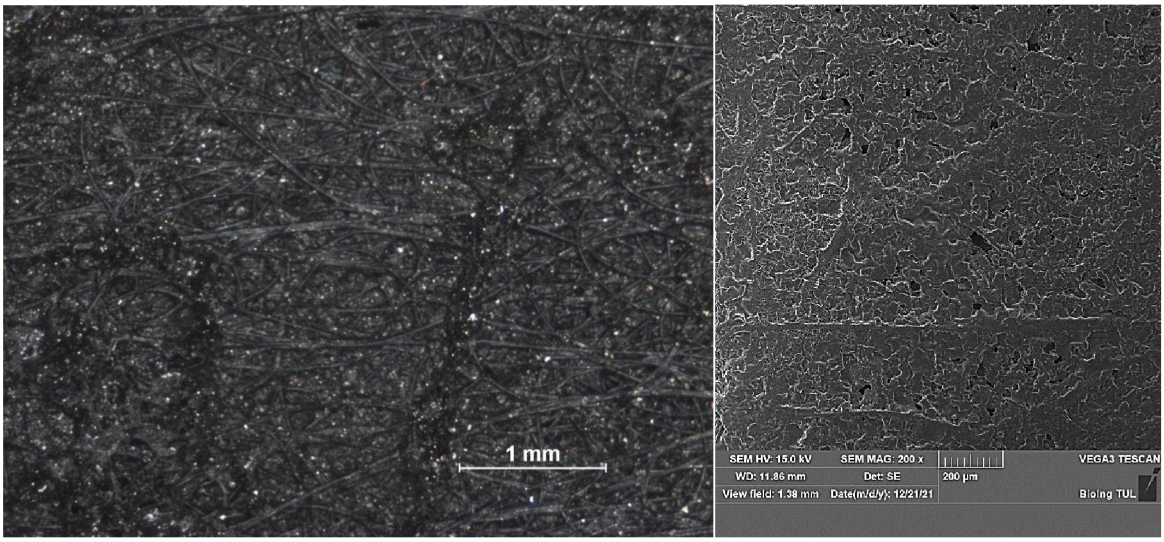

Figure 31: Sample 7 (Left) Optical microscope image (Right) SEM image

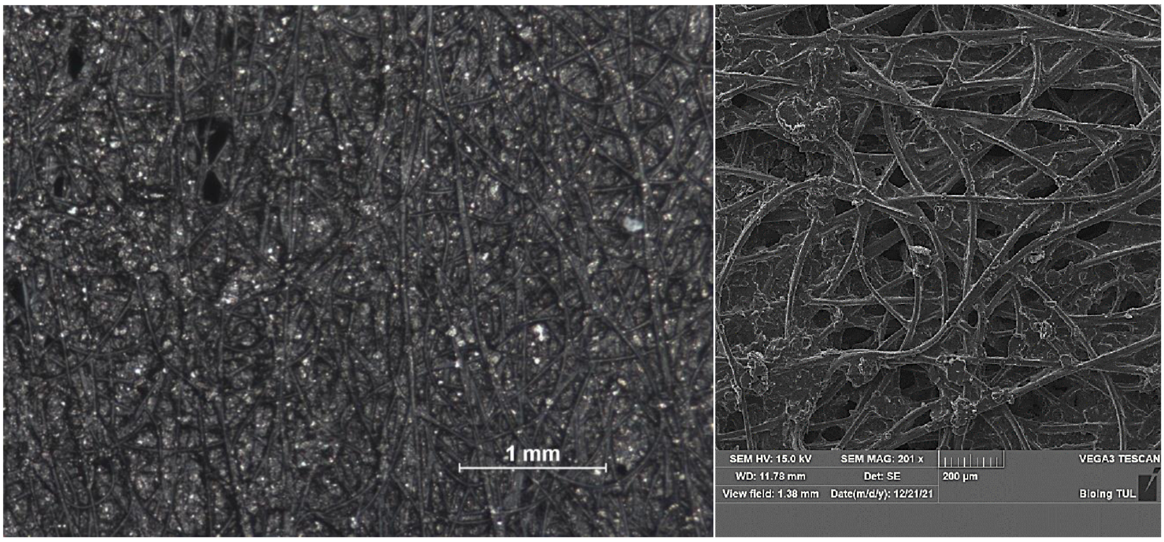

Figure 32: Sample 8 (Left) Optical microscope image (Right) SEM image

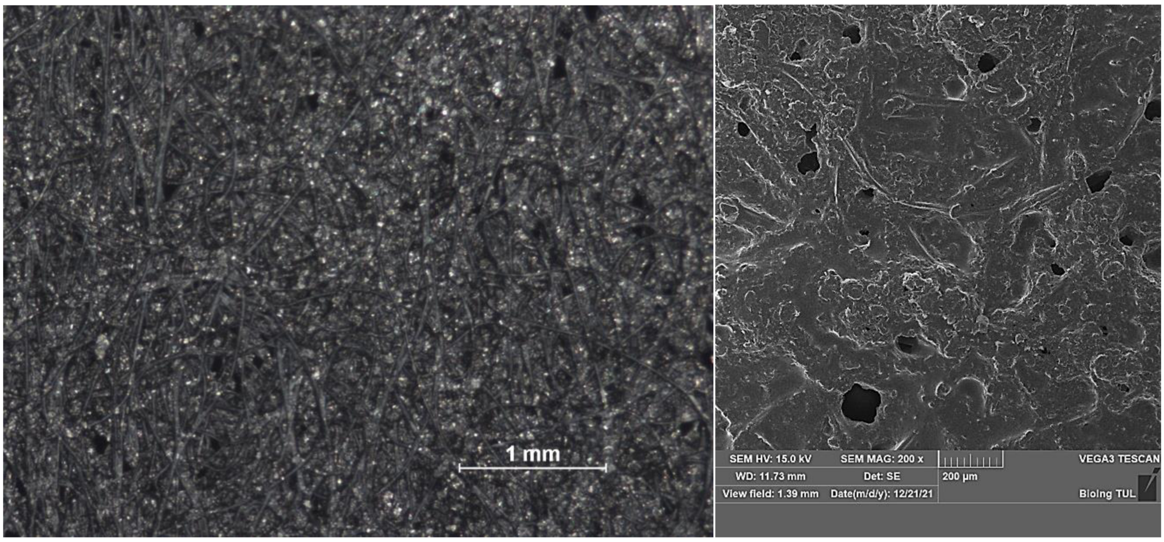

Figure 33: Sample 9 (Left) Optical microscope image (Right) SEM image

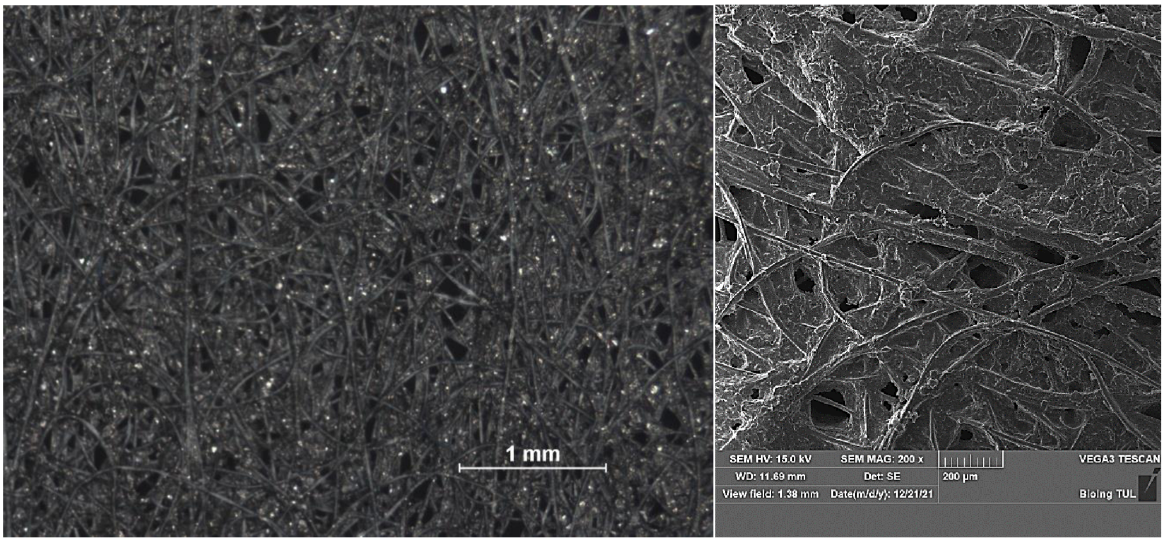

Figure 34: Sample 10 (Left) Optical microscope image (Right) SEM image

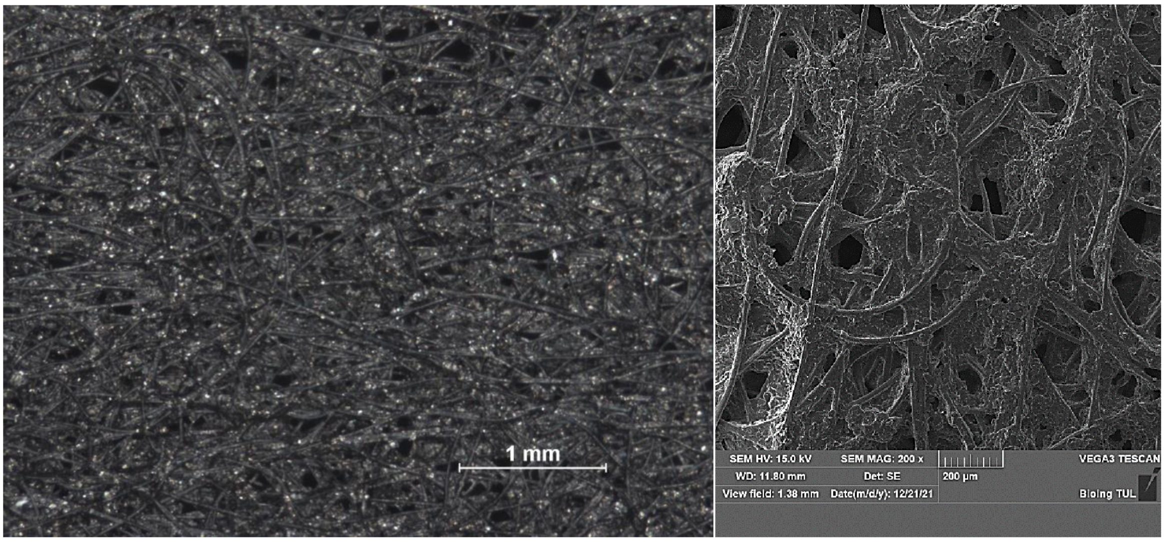

Figure 35: Sample 11 (Left) Optical microscope image (Right) SEM image

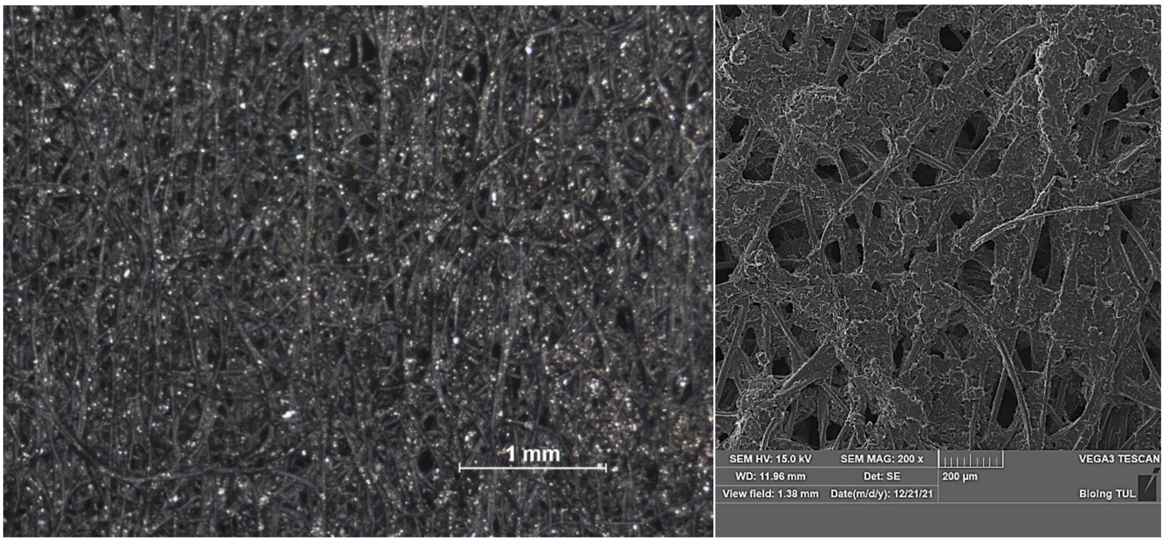

Figure 36: Sample 12 (Left) Optical microscope image (Right) SEM image

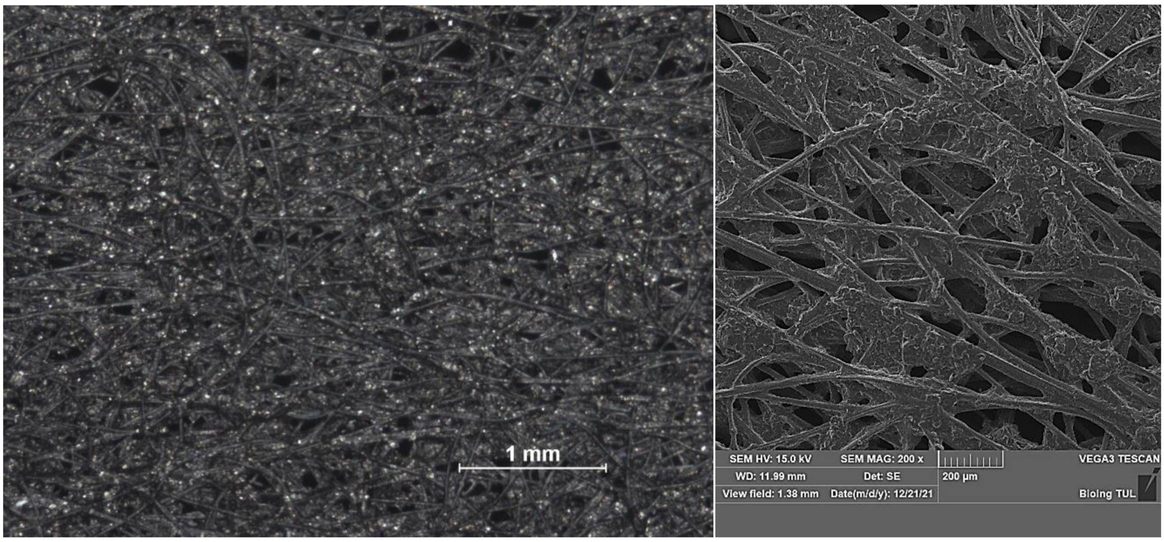

Figure 37: Sample 13 (Left) Optical microscope image (Right) SEM image

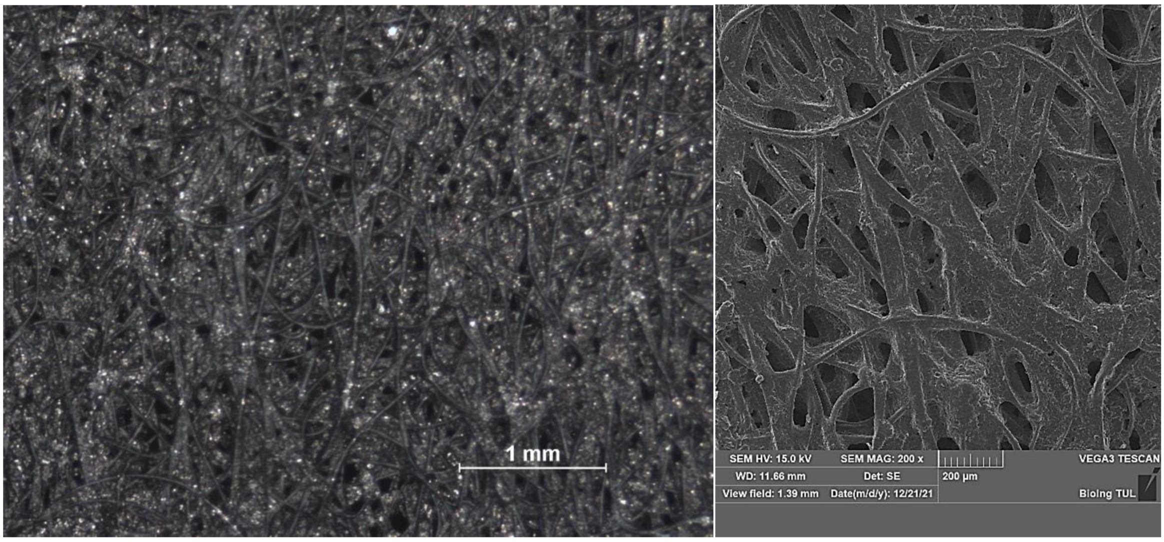

Figure 38: Sample 14 (Left) Optical microscope image (Right) SEM image

The optical microscope images illustrate how well the fibres were coated with the composite over a large area as well its penetration into the structure of the material. SEM analysis indicated the deposition of composite onto the viscose fibres and its agglomeration. From the images it was concluded that the textile fibres were well coated with the composite. Increase in filler concentration indicated a higher degree of filler incorporation onto the fibres as seen by the increase in fibre darkness by optical microscopy images. This is supported by the measurement data in table 7 as more carbon was incorporated onto the textile with increase in filler concentration. This would suggest that the coating had a great affinity towards the viscose fibres to incorporate the filler onto the textile. All optical images indicated areas where the structure of the coated material remained open. This is seen where the direct light from the microscope penetrated the structures. This was due to the nature of the open structure of the nonwoven material resulting in the open spaces. Smaller spaces in the structure were filled with coating agglomeration which connected individual fibres. It was therefore concluded that the cover of the coating is dependent on the structure of the material to which the coating is applied. From the optical microscope image in figure 30 it was determined that the coating containing spherical graphite was present in lesser quantity and less uniformly on the textile compared to graphene containing samples. This is indicated by the light-coloured spaces on the textile. This observation was also supported by the low weight of coating applied as indicated in table 7. From this observation it would suggest that there is less contact between particles in sample 6. This resulted in an increased percolation threshold for the sample compared to sample 5. Sample 5 had the same filler content as sample 6 although the larger graphene particles were used. The graphene filler was much more present on the viscose fibres, as illustrated in figure 29. This should suggest a lower percolation threshold for the larger filler particle. It was determined from the SEM images that particle agglomeration increased with increase in filler content. This could be attributed to the hydrophobic nature of the particles resulting in particle agglomeration. Non-ionic surfactant, decyl glucoside, was used to overcome the problem during particle mixing. It improved sample preparation, however agglomeration still occurred on the textile.

7.5.Crosslink strength (MEK) test

It was determined that a sample which was cured at 120 °C was the only sample to successfully satisfy the testing conditions. No damage was evident when conducting the test and it was assumed that the sample would have withstood even further testing. The reason for the increase in curing temperature compared to the 40 °C -70 °C stated in literature could be attributed to the addition of water to the system. This would explain the curing temperature of >100 °C which would correspond to the temperature at which water evaporates. It is possible that at the lower curing temperature could be used if less water was added to the system or if curing was taking place over a longer period [9]. For all samples produced the MEK solvent rub test was repeated with unchanged results.

7.6.Measurement of electrical properties

The volume electrical resistivity of the graphene powder was calculated according to equation 4 to be 10.21 ± 2.16 Ω.cm. Similarly, the volume electrical resistivity for the finer spherical graphite was calculated to be 13.13 ± 0.41 Ω.cm. Measurement data for the electrical volume resistivity of the powder samples are illustrated in table 8 in the appendix. Measurement data for the surface- and volume electrical resistivity of the coated samples are respectively illustrated in tables 9 and 10 in the appendix. Figures 39 and 40 illustrates the relationship between the surface and volume resistivity with respect to the graphene filler content of each sample respectively. Figure 41 illustrates the ratio of the surface and volume resistivity with respect to the graphene filler content. The results are for samples 1-5, 7-10 and 12 which all contain graphene filler with no surfactant used during processing or double layering. For all samples measured the statistical analysis is presented in the appendix.

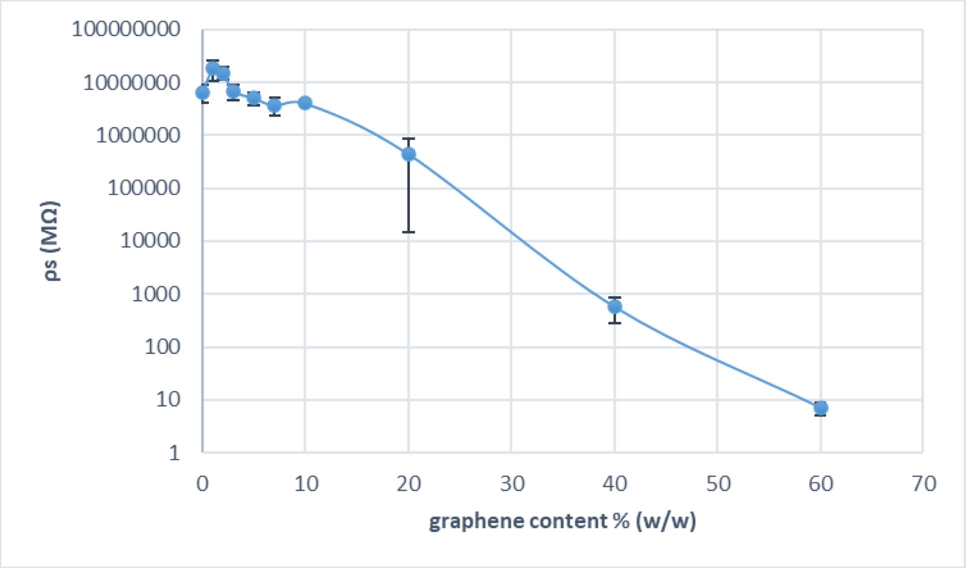

Figure 39: Surface electrical resistivity as a function of graphene content in liquid coating (samples prepared without surfactant)

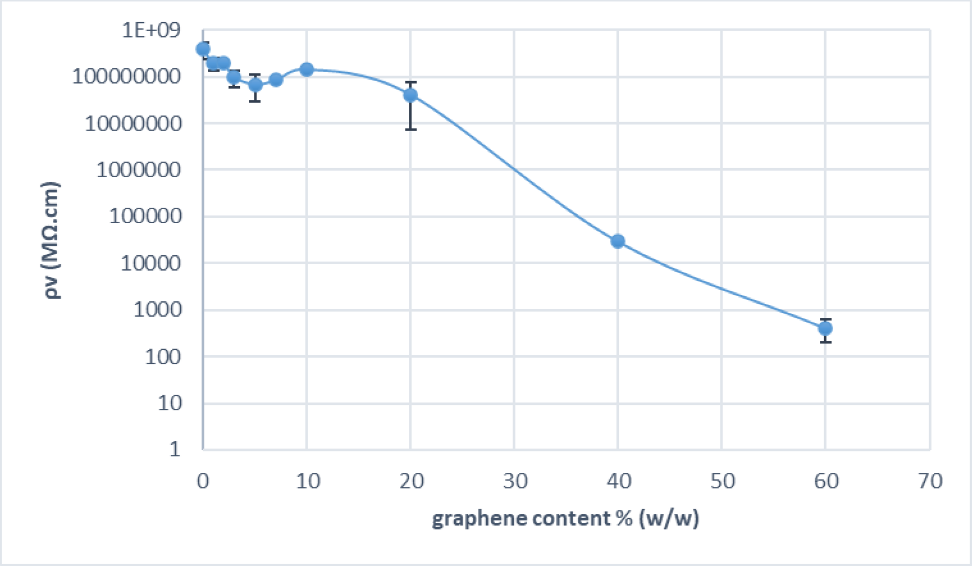

Figure 40: Volume electrical resistivity as a function of graphene content in liquid coating (samples prepared without surfactant)

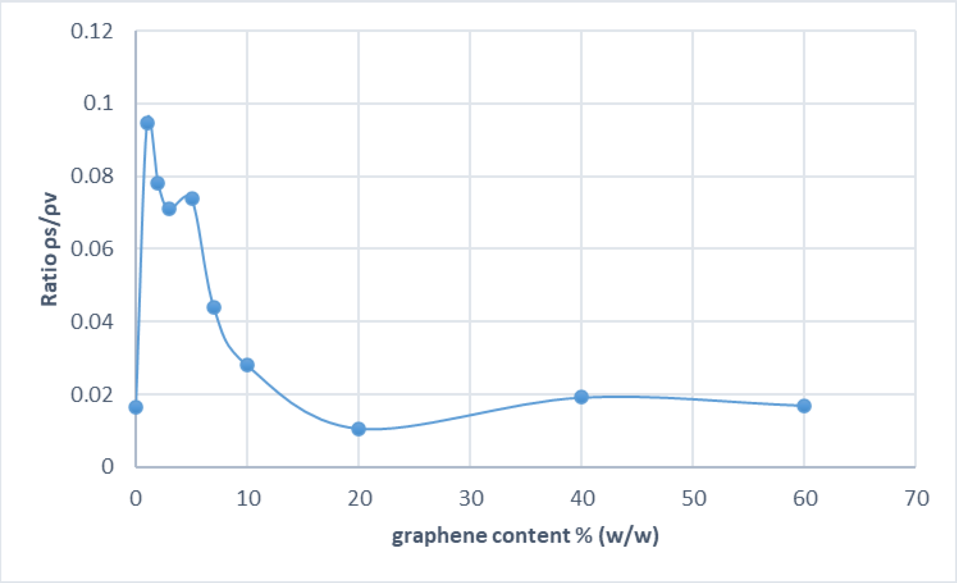

Figure 41: Ratio of ρs/ρv as a function of graphene content in liquid coating (samples prepared without surfactant)

The graphs in figures 39 and 40 indicated that there is a direct relationship between the surface and volume electrical resistivity of the samples. The volume electrical resistivity was higher for all samples indicating that most of the filler materials were deposited on the surface of the structures. This resulted in more conductive pathways formed on the surface of the viscose than within the structure. With an increase in filler content the electrical resistivity decreased significantly by up to a factor of 10^6. The percolation threshold was determined to be around 30 % of graphene filler content using sample preparation method 2. This was concluded since the electrical resistivity increased exponentially before this point and started to plateau after. It was determined that the finer particle used in sample 6 could exhibit a greater percolation threshold. This was concluded since at the same particle loading, the surface electrical resistivity of sample 5 was 10.50 % lower and the volume electrical resistivity 56.36% lower than that of sample 6. As illustrated in figure 41, the surface to volume electrical resistivity ratio is higher for samples which contained lower amount of filler. This can be attributed to more particle agglomeration on the surface of the textile at higher filler content resulting in a lower electrical resistivity on the textile surface compared to within the textile structure.

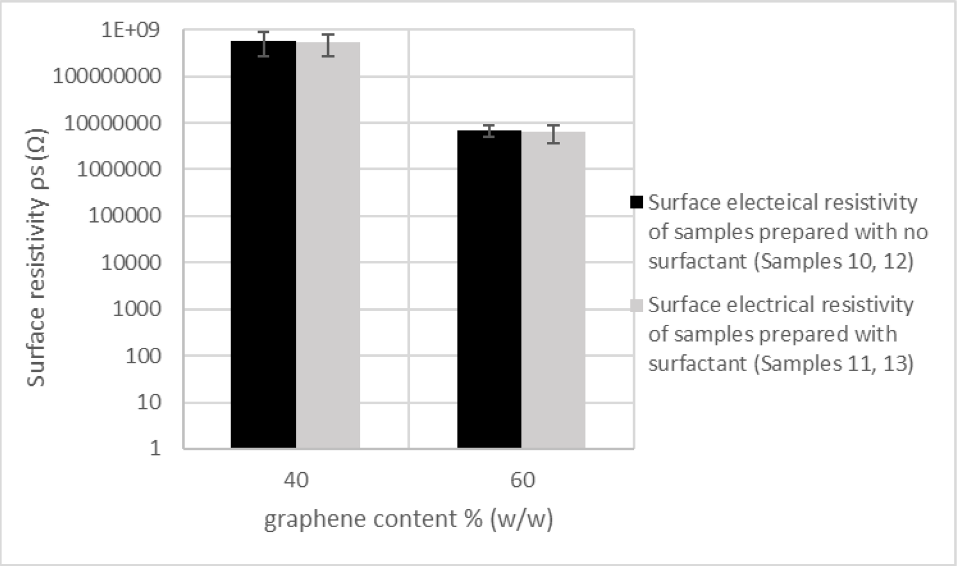

Figure 42: Surface resistivities of samples 10, 11 (40 %) and samples 12, 13 (60 %)

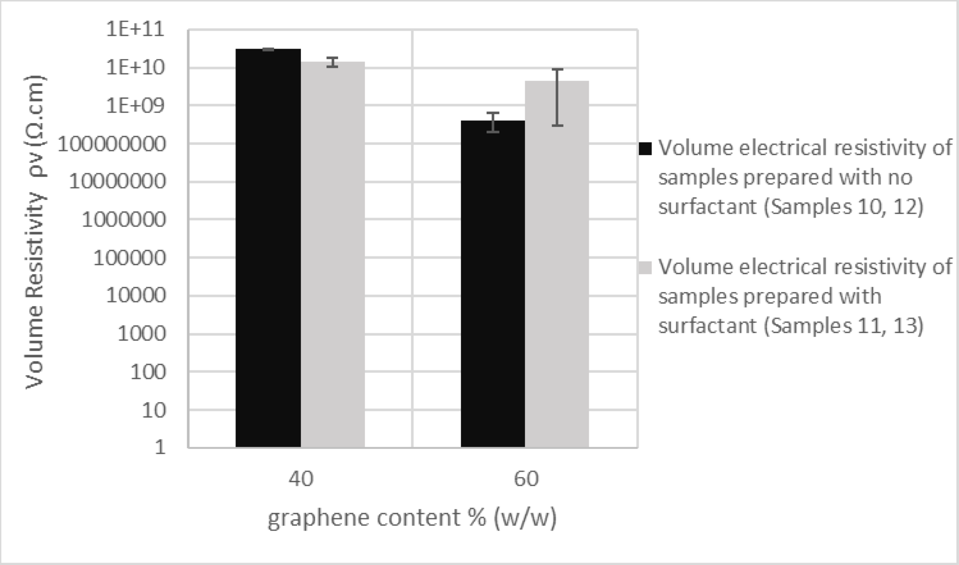

Figure 43: Volume resistivities of samples 10, 11 (40 %) and samples 12, 13 (60 %)

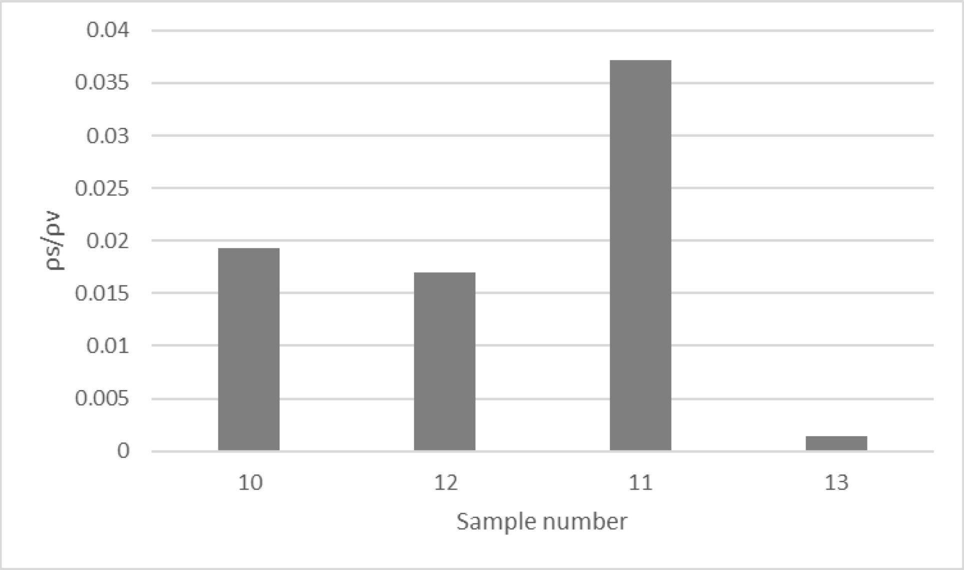

Figure 44: Ratio of ρs/ρv for comparing samples prepared with and without surfactant

Figures 42 and 43 illustrates the differences in surface and volume electrical resistivities of samples 10 and 12 which were produced with no surfactant and samples 11 and 13 which were produced with surfactant. The purpose of the surfactant was to decrease the surface energy of the filer particles to promote effective mixing by overcoming particle agglomeration. It can be seen in figures 34-37 that there were no significant differences in particle dispersion or change in particle agglomeration on the fibres. This observation is supported by the electrical resistivity measurements since there were small differences in electrical resistivity measured. It appeared initially as if the samples 11 and 13 performed slightly better indicating that the addition of surfactant was beneficial; however, the volume resistivity of sample 13 was higher by a factor of 10^1. When taking the 95% confidence interval into consideration it was concluded that the mean resistivity values were comparable. This would suggest that the use of decyl glucoside surfactant had no measurable impact on the electrical resistivity of the materials produced. The electrical properties were mainly impacted by filler content. Figure 44 illustrates the relationships between the surface and volume electrical resistivity ratios of the respective samples. There ρs/ρv ratios for samples 10,12, 11 and 13 were 0.0193, 0.0170, 0.0371, 0.0014 respectively. The lowest value was obtained for sample 13 which would suggest that the sample had a higher electrical conductivity on the surface of the material compared to within the structure. Sample 11 with a ρs/ρv ratio of 0.0371 was the best performer of the compared samples since it exhibited less electrical resistivity throughout the structure. The results indicated no clear relationship between samples which were prepared with surfactant and those without. The only observable trend was that the ρs/ρv ratio decreased with increased filler content as previously stated for samples non surfactant containing samples.

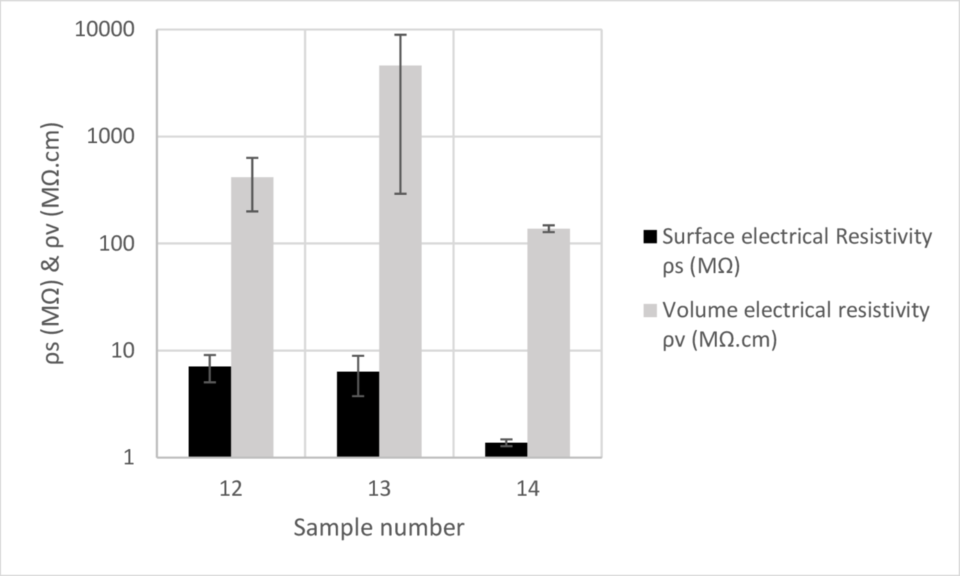

Figure 45: Electrical properties of samples containing 60% graphene filler with different processing conditions

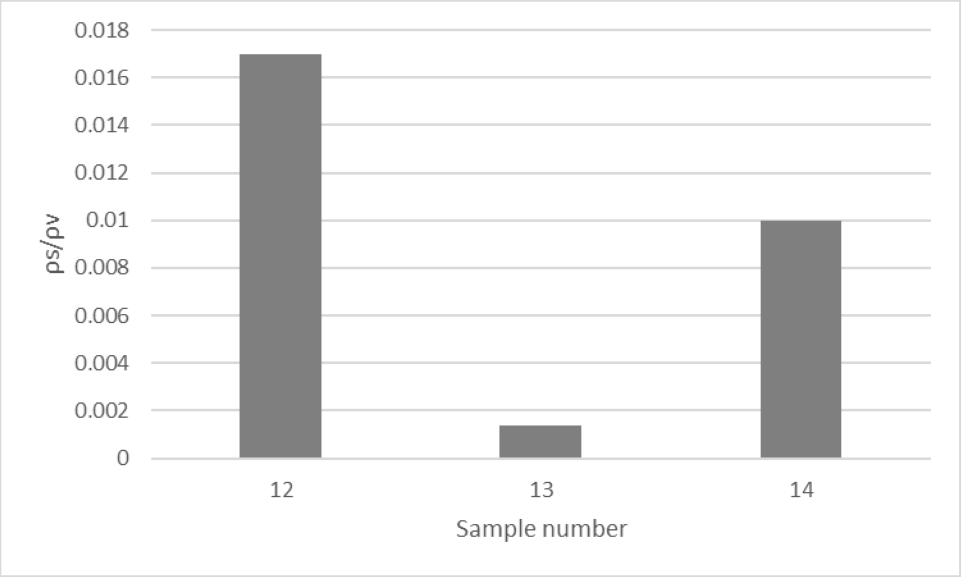

Figure 46: Ratio ρs/ρv for samples containing 60% graphene filler with different processing conditions

Figure 45 illustrates the difference in surface and volume electrical resistivities between single layer samples 12, 13 and sample 14 which was produced by double coating the textile material. The coating used also contained decyl glucoside surfactant as used to produce sample 13. Double layering of the composite proved to be more effective since the surface resistivity of sample 14 was 80.48% and 78.24% lower than that of samples 12 and 13 respectively. The volume resistivity of sample 14 was 66.83% and 97.01% lower than that of samples 12 and 13 respectively. As illustrated in figure 46 the ρs/ρv ratios were determined to be 0.0170, 0.0014, 0.0100 for samples 12,13 and 14 respectively. Sample 14 had a comparable surface to volume electrical resistivity ratio to other samples; indicating that there was no significant improvement in electrical resistivity within the structure of the material compared to the surface. Since it was previously established that the use of the surfactant had no influence over the electrically conductive properties of the material it can be concluded that double layering of the composite on the textile significantly improved the electrical conductivity of the material.

7.7.Measurement of EMI shielding effectiveness

All samples were measured for their EMI shielding over a measurement range of 30 MHz – 3 GHz. None of the samples exhibited any EMI shielding properties over the measured frequency range. This can be attributed to the low electrical conductivity of the samples compared to that of highly orientated carbon structures used as filling material in previous studies. Composite materials containing carbon fillers for EMI shielding are typically thin membranes which allow for better in-plane particle to particle contact with a more efficient network structure [41–44]. It is possible that EMI shielding could occur at higher frequencies, however the tested range was limited by the equipment used.

8. Conclusion

The volume electrical resistivity of the graphene powder was determined to be 10.21 ± 2.16 Ω.cm. and 13.13 ± 0.41 Ω.cm for the spherical graphite powder. It was determined from the SEM image of the larger graphene particles (figure 23) that it more closely resembled graphite compared to graphene. This made the particles more comparable since the difference was mainly due to particle size. The lower electrical resistivity of the larger particles was attributed to the decrease in particle grain boundary resulting in an increase in electrical conductivity. This statement is supported by observations made in the studies of Nagata et al. and Liu et al. The sample thickness was directly related to the amount of coating applied to the textile. Sample preparation method 2 was concluded to be the most practical method due to its scalability and improved consistency of coating application compared to sample preparation method 1. Using DSC (figure 19) it was concluded that the textile material used was viscose due to the absence of polymeric material as well as the observed degradation. This was confirmed by polarised light optical microscopy which indicated a fibre type visually corresponding to that of viscose due to the expected cross-sectional shape (figure 25). It was determined that the glass transition temperature for the coating system corresponded well with what is stated in the literature. The endothermic peaks observed in figures 20 and 22 was suggested to due to crosslink chain movement/degradation at the polymer-textile and polymer-filler interface. Using optical transmission microscopy, SEM and the MEK solvent rub test it was concluded that the developed coating had an excellent affinity towards viscose fibres. It was concluded that the smaller filler particles exhibited a higher percolation threshold compared to the larger particles due to higher electrical resistance at similar particle loading. This observation was like the findings of Marinho et al. and Nagata et al. where particle to particle contact had a greater effect on the electrical conductivity of the samples using larger filler particles compared to smaller spherical graphite. Thus, the observations of this work as well as the forementioned is opposite to the findings of Chen et al. Increase in filler concentration resulted in less electrical resistivity and greater particle agglomeration. It was also evident during processing that the increase in filler content resulted in an increase in viscosity of the coating as well as particle agglomeration during mixing. Although during processing the addition of decyl glucoside indicated less particle agglomeration during mixing. It was determined that the addition of the surfactant had minimal effect on the particle agglomeration after coating. There was also no observable trend difference in the electrical resistivity when comparing samples which were prepared with and without surfactant. It was concluded that layering of the coating after curing of subsequent layers would be very effective at improving the electrical conductivity of the samples. None of the samples exhibited any effective EMI shielding. This was attributed to the relatively low electrical conductivities of the materials produced as well as the low frequency test range of 30 MHz – 3 GHz. The lower electrical conductivity of the samples produced could be attributed to less in-plane particle contact given the anisotropic nature of graphite materials. It is therefore suggested that improvements can be made by using a method of lamination rather than a dipping or padding application. It is suggested that friction padding could produce a sample which is more conductive due to better in plane particle contact in the applied coating. It is believed that a thinner coating would promote more in-plane particle to particle contact resulting in an increase in electrical conductivity.

The produced materials exhibited a very low electrical conductivity and can be considered as mostly antistatic. Its advantage is that the coating allows the material to be relatively flexible in ambient conditions. Its main disadvantage is that there are cheaper alternatives with greater electrical properties. The material is also only available in black due to the presence of carbon the surface. With an improvement in electrical conductivity the material could be used in flexible electronics such as smart clothing.

References

[1] TITIRICI, Maria Magdalena, Robin J. WHITE, Nicolas BRUN, Vitaliy L. BUDARIN, Dang Sheng SU, Francisco DEL MONTE, James H. CLARK a Mark J. MACLACHLAN. Sustainable carbon materials. *Chemical Society Reviews* [online]. 2015, **44**(1), 250–290. ISSN 14604744. Dostupné z: doi:10.1039/c4cs00232f

[2] CHUNG, D. D.L. Review: Graphite. *Journal of Materials Science* [online]. 2002, **37**(8), 1475–1489. ISSN 00222461. Dostupné z: doi:10.1023/A:1014915307738

[3] GONZALEZ CARMONA, Juan Manuel, Alexander RUDEN MUÑOZ, Christian BARBOSA, Carolina ORTEGA PORTILLA a Federico SEQUEDA OSORIO. Computational Study of Allotropic Structures of Carbon by Density Functional Theory (DTF). *Ingeniería y Ciencia* [online]. 2014, **10**(19), 145–162. ISSN 17949165. Dostupné z: doi:10.17230/ingciencia.10.19.7

[4] FREDRIKSSON, Tore. *Carbon Nanotubes : A Theoretical study of Young's modulus*. B.m., 2014. Karlstads University.

[5] XIAO, Jinkun, Lei ZHANG, Kechao ZHOU, Jianguo LI, Xinlin XIE a Zhiyou LI. Anisotropic friction behaviour of highly oriented pyrolytic graphite. *Carbon* [online]. 2013, **65**, 53–62. ISSN 00086223. Dostupné z: doi:10.1016/j.carbon.2013.07.101

[6] SHUAI, Shirong, Yu LIU, Cong ZHAO, Hongyu ZHU, Yang LI, Kanghong ZHOU, Wei GE a Jianyuan HAO. Improved synthesis of graphene oxide with controlled oxidation degree by using different dihydrogen phosphate as intercalators. *Chemical Physics* [online]. 2020, **539**(April), 110938. ISSN 03010104. Dostupné z: doi:10.1016/j.chemphys.2020.110938

[7] TAHERIAN, Reza. Experimental and analytical model for the electrical conductivity of polymer-based nanocomposites. *Composites Science and Technology* [online]. 2016, **123**, 17–31. ISSN 02663538. Dostupné z: doi:10.1016/j.compscitech.2015.11.029

[8] COETZEE, Divan, Mohanapriya VENKATARAMAN, Jiri MILITKY a Michal PETRU. Influence of Nanoparticles on Thermal and Electrical Conductivity of Composites. *Polymers* [online]. 2020, **12**(4), 742. Dostupné z: doi:10.3390/polym12040742

[9] MASNÁ, Anežka. *Textilní kompozity z přírodních vláken Bakalářská práce* [online]. B.m., 2018. Technical Unversity of Liberec. Dostupné z: https://dspace.tul.cz/handle/15240/32197

[10] HAMDY, Louise B., Russell J. WAKEHAM, Marco TADDEI, Andrew R. BARRON a Enrico ANDREOLI. Epoxy Cross-Linked Polyamine CO2 Sorbents Enhanced via Hydrophobic Functionalization. *Chemistry of Materials* [online]. 2019, **31**(13), 4673–4684. ISSN 15205002. Dostupné z: doi:10.1021/acs.chemmater.9b00574

[11] ROMÁN, Frida, Pere COLOMER, Yolanda CALVENTUS a John M. HUTCHINSON. Study of hyperbranched poly(ethyleneimine) polymers of different molecular weight and their interaction with epoxy resin. *Materials* [online]. 2018, **11**(3), 1–26. ISSN 19961944. Dostupné z: doi:10.3390/ma11030410

[12] LIU, Haitao a Lei LI. Graphitic materials: Intrinsic hydrophilicity and its implications. *Extreme Mechanics Letters* [online]. 2017, **14**, 44–50. ISSN 23524316. Dostupné z: doi:10.1016/j.eml.2017.01.010

[13] LITVIN, D B a V KOPSKY. *International Tables for Crystallography* [online]. 1. vyd. Dordrecht: Springer, 2006. Dostupné z: doi:10.1107/97809553602060000107

[14] HOWE, J. Y., C. J. RAWN, L. E. JONES a H. OW. Improved crystallographic data for graphite. *Powder Diffraction* [online]. 2003, **18**(2), 150–154. ISSN 0885-7156. Dostupné z: doi:10.1154/1.1536926

[15] MU, Ulrich. International Tables for Crystallography, Volume A, Space-group symmetry . 6th edition. Edited by Mois I. Aroyo. Wiley, 2016. Pp. xxi + 873. *Acta Crystallographica Section A Foundations and Advances* [online]. 2016, **73**(3), 873. Dostupné z: http://scripts.iucr.org/cgi-bin/paper?S2053273317005526

[16] ARORA, Mallika, Sergio PINEDA, P Andrew WILLIAMS, Kenneth D M HARRIS a Benson M KARIUKI. Polymorphic Adaptation. In: *17th International Conference,CAAD Futures*. Istanbul, Turkey: CumInCAD, 2017, s. 474–491.

[17] TANZI, Maria Cristina, Silvia FARÈ a Gabriele CANDIANI. *Organization, Structure, and Properties of Materials* [online]. 1. vyd. B.m.: Academic Press, 2019. ISBN 9780081010341. Dostupné z: doi:10.1016/b978-0-08-101034-1.00001-3

[18] SCHNEIDER, Johannes M. *ELECTRONIC PROPERTIES OF GRAPHITE* [online]. B.m., 2010. Grenoble ; Université Joseph-Fourier - Grenoble I. Dostupné z: https://tel.archives-ouvertes.fr/tel-00547304

[19] GUINEA, F., A. H. CASTRO NETO a N. M.R. PERES. Electronic properties of stacks of graphene layers. *Solid State Communications* [online]. 2007, **143**(1–2), 116–122. ISSN 00381098. Dostupné z: doi:10.1016/j.ssc.2007.03.053

[20] BURLATSKY, Sergei F., Vadim V. ATRAZHEV, Dmitry V. DMITRIEV, Vadim I. SULTANOV, Elena N. TIMOKHINA, Elena A. UGOLKOVA, Sonia TULYANI a Antonio VINCITORE. Surface tension model for surfactant solutions at the critical micelle concentration. *Journal of Colloid and Interface Science* [online]. 2013, **393**(1), 151–160. ISSN 00219797. Dostupné z: doi:10.1016/j.jcis.2012.10.020

[21] ISHIBASHI, Ayumi a Naotoshi NAKASHIMA. Individual dissolution of single-walled carbon nanotubes in aqueous solutions of steroid or sugar compounds and their Raman and near-IR spectral properties. *Chemistry - A European Journal* [online]. 2006, **12**(29), 7595–7602. ISSN 09476539. Dostupné z: doi:10.1002/chem.200600326

[22] CORTÉS, Hernán, Héctor HERNÁNDEZ-PARRA, Sergio A. BERNAL-CHÁVEZ, María L. DEL PRADO-AUDELO, Isaac H. CABALLERO-FLORÁN, Fabiola V. BORBOLLA-JIMÉNEZ, Maykel GONZÁLEZ-TORRES, Jonathan J. MAGAÑA a Gerardo LEYVA-GÓMEZ. Non-ionic surfactants for stabilization of polymeric nanoparticles for biomedical uses. *Materials* [online]. 2021, **14**(12), 1–39. ISSN 19961944. Dostupné z: doi:10.3390/ma14123197

[23] BACCILE, Niki, Chloé SEYRIG, Alexandre POIRIER, Silvia ALONSO-DE CASTRO, Sophie L.K.W. ROELANTS a Stéphane ABEL. Self-assembly, interfacial properties, interactions with macromolecules and molecular modelling and simulation of microbial bio-based amphiphiles (biosurfactants). A tutorial review. *Green Chemistry* [online]. 2021, **23**(11), 3842–3944. ISSN 14639270. Dostupné z: doi:10.1039/d1gc00097g

[24] QIN, Jie, Jian QU, Yanwen LI, Bo WANG, Zhipeng SUN, Hongqiang ZHANG a Weidong ZHANG. Mechanical properties of highly dispersed carbon nanotubes reinforced cement-based materials. *{IOP} Conference Series: Materials Science and*

Engineering [online]. 2019, **569**(2), 22025. Dostupné z: doi:10.1088/1757-899x/569/2/022025

[25] SIS, H a M BIRINCI. Effect of nonionic and ionic surfactants on zeta potential and dispersion properties of carbon black powders. *Colloids and Surfaces A: Physicochemical and Engineering Aspects* [online]. 2009, **341**(1), 60–67. ISSN 0927-7757. Dostupné z: doi:https://doi.org/10.1016/j.colsurfa.2009.03.039

[26] NERUDA, Marek. *Modelling of electrical resistivity for electrically conductive textile*. B.m., 2014. Czech Technical University in Prague.

[27] CHEN, Guo Hua, Da Jun WU, Wen Gui WENG a Wen Li YAN. Dispersion of graphite nanosheets in a polymer matrix and the conducting property of the nanocomposites. *Polymer Engineering and Science* [online]. 2001, **41**(12), 2148–2154. ISSN 00323888. Dostupné z: doi:10.1002/pen.10909

[28] ABDEL AZIZ, Ahmed A., Ali T. ABDEL-MOTAGALY, Ahmed A. IBRAHIM, Waleed M.A. EL ROUBY a Mahmoud A. ABDALLA. A printed expanded graphite paper based dual band antenna for conformal wireless applications. *AEU - International Journal of Electronics and Communications* [online]. 2019, **110**, 152869. ISSN 16180399. Dostupné z: doi:10.1016/j.aeue.2019.152869

[29] HUANG, Xingyi, Fei LIU, Pingkai JIANG a Toshikatsu TANAKA. Is graphene oxide an insulating material? *Proceedings of IEEE International Conference on Solid Dielectrics, ICSD* [online]. 2013, 904–907. ISSN 15535282. Dostupné z: doi:10.1109/ICSD.2013.6619690

[30] KAUSAR, Ayesha. Poly(methyl methacrylate) nanocomposite reinforced with graphene, graphene oxide, and graphite: a review. *Polymer-Plastics Technology and Materials* [online]. 2019, **58**(8), 821–842. ISSN 2574089X. Dostupné z: doi:10.1080/25740881.2018.1563112

[31] CAO, Qing, Shu Jen HAN, Jerry TERSOFF, Aaron D. FRANKLIN, Yu ZHU, Zhen ZHANG, George S. TULEVSKI, Jianshi TANG a Wilfried HAENSCH. End-bonded contacts for carbon nanotube transistors with low, size-independent resistance. *Science* [online]. 2015, **350**(6256), 68–72. ISSN 10959203. Dostupné z: doi:10.1126/science.aac8006

[32] AL-SOLAMY, Falleh R., A. A. AL-GHAMDI a Waleed E. MAHMOUD.

Piezoresistive behavior of graphite nanoplatelets based rubber nanocomposites. *Polymers for Advanced Technologies* [online]. 2012, **23**(3), 478–482. ISSN 10427147. Dostupné z: doi:10.1002/pat.1902

[33] MARINHO, Bernardo, Marcos GHISLANDI, Evgeniy TKALYA, Cor E. KONING a Gijsbertus DE WITH. Electrical conductivity of compacts of graphene, multi-wall carbon nanotubes, carbon black, and graphite powder. *Powder Technology* [online]. 2012, **221**, 351–358. ISSN 00325910. Dostupné z: doi:10.1016/j.powtec.2012.01.024

[34] SONG, Rongguo, Qianlong WANG, Boyang MAO, Zhe WANG, Danli TANG, Bin ZHANG, Jingwei ZHANG, Chengguo LIU, Daping HE, Zhi WU a Shichun MU. Flexible graphite films with high conductivity for radio-frequency antennas. *Carbon* [online]. 2018, **130**, 164–169. ISSN 00086223. Dostupné z: doi:10.1016/j.carbon.2018.01.019

[35] NAGATA, Kazuya, Hitoshi IWABUKI a Hideyuki NIGO. Effect of particle size of graphites on electrical conductivity of graphite/polymer composite. *Composite Interfaces* [online]. 1999, **6**(5), 483–495. ISSN 15685543. Dostupné z: doi:10.1163/156855499X00161

[36] LIU, Ben, Dongqing ZHANG, Xiangfen LI, Zhao HE, Xiaohui GUO, Zhanjun LIU a Quangui GUO. Effect of graphite flakes particle sizes on the microstructure and properties of graphite flakes/copper composites. *Journal of Alloys and Compounds* [online]. 2018, **766**, 382–390. ISSN 09258388. Dostupné z: doi:10.1016/j.jallcom.2018.06.129

[37] ALOFI, A. a G. P. SRIVASTAVA. Thermal conductivity of graphene and graphite. *Physical Review B - Condensed Matter and Materials Physics* [online]. 2013, **87**(11), 1–10. ISSN 10980121. Dostupné z: doi:10.1103/PhysRevB.87.115421

[38] AYAD, Neveen M., Hala A. BAHGAT, Eman Hussain AL KABA a Maryam Hussain BUHOLAYKA. Food simulating organic solvents for evaluating crosslink density of bulk fill composite resin. *International Journal of Dentistry* [online]. 2017, **2017**. ISSN 16878736. Dostupné z: doi:10.1155/2017/1797091

[39] ŠAFÁŘOVÁ, Veronika a Jiří MILITKÝ. Electromagnetic shielding properties of woven fabrics made from high-performance fibers. *Textile Research Journal*

[online]. 2014, **84**(12), 1255–1267. ISSN 17467748. Dostupné z: doi:10.1177/0040517514521118

[40] ACEBO, Cristina, Xavier RAMIS a Angels SERRA. Improved epoxy thermosets by the use of poly(ethyleneimine) derivatives. *Physical Sciences Reviews* [online]. 2017, **2**(8), 1–31. ISSN 2365659X. Dostupné z: doi:10.1515/psr-2016-0128

[41] SONG, Ping, Chaobo LIANG, Lei WANG, Hua QIU, Hongbo GU, Jie KONG a Junwei GU. Obviously improved electromagnetic interference shielding performances for epoxy composites via constructing honeycomb structural reduced graphene oxide. *Composites Science and Technology* [online]. 2019, **181**, 107698. ISSN 0266-3538. Dostupné z: doi:https://doi.org/10.1016/j.compscitech.2019.107698

[42] SONG, Wei-Li, Mao-Sheng CAO, Ming-Ming LU, Song BI, Chan-Yuan WANG, Jia LIU, Jie YUAN a Li-Zhen FAN. Flexible graphene/polymer composite films in sandwich structures for effective electromagnetic interference shielding. *Carbon* [online]. 2014, **66**, 67–76. ISSN 0008-6223. Dostupné z: doi:https://doi.org/10.1016/j.carbon.2013.08.043

[43] YAN, Ding-Xiang, Huan PANG, Bo LI, Robert VAJTAI, Ling XU, Peng-Gang REN, Jian-Hua WANG a Zhong-Ming LI. Structured Reduced Graphene Oxide/Polymer Composites for Ultra-Efficient Electromagnetic Interference Shielding. *Advanced Functional Materials* [online]. 2015, **25**(4), 559–566. Dostupné z: doi:https://doi.org/10.1002/adfm.201403809

[44] YU, Zhi, Tianwen DAI, Shuaiwei YUAN, Huawei ZOU a Pengbo LIU. Electromagnetic Interference Shielding Performance of Anisotropic Polyimide/Graphene Composite Aerogels. *ACS Applied Materials \& Interfaces* [online]. 2020, **12**(27), 30990–31001. Dostupné z: doi:10.1021/acsami.0c07122

Appendix

Statistical analysis was performed using descriptive statistics in the excel data analysis tool pack.

Electrical resistivity measurement results

Table 8: Carbon powder electrical resistivity measurements

	Graphene Electrical resistance (Ω)	**Graphene electrical volume resistivity (Ω.cm)**	**Sphericle graphite electrical resistance (Ω)**	**Sphericle graphite electrical volume resistivity (Ω.cm)**
measurement	1.14	8.91	2.08	13.61
	1.59	12.49	2.00	13.07
	1.49	11.70	2.03	13.29
	1.14	8.93	1.97	12.91
	1.15	9.03	1.95	12.78
Average	1.30	**10.21**	2.01	**13.13**
Compact powder thickness (cm)	0.10		0.12	

Table 9: Surface electrical resistivity of samples as listed in table 7

Sample	**Untreated**	**1**	**2**	**3**	**4**	**5**	**6**	**7**	**8**
Carbon content (%)	no coating	0	1	2	3	5	5	7	10
Measurements	3.42E+13	9.78E+12	2.48E+13	1.32E+13	8.23E+12	6.35E+12	4.53E+12	5.41E+12	4.05E+12
	1.55E+13	5.59E+12	2.46E+13	2.10E+13	5.50E+12	4.82E+12	5.85E+12	4.20E+12	4.55E+12
	2.72E+13	5.42E+12	1.30E+13	1.51E+13	9.39E+12	5.40E+12	8.02E+12	3.02E+12	3.93E+12
	2.20E+13	5.94E+12	1.80E+13	1.27E+13	6.24E+12	5.65E+12	5.27E+12	3.07E+12	3.84E+12
	1.55E+13	5.43E+12	1.12E+13	1.39E+13	5.26E+12	3.26E+12	4.79E+12	2.71E+12	3.87E+12
Surface Resistivity ρs (Ω)	2.29E+13	6.43E+12	1.83E+13	1.52E+13	6.93E+12	5.09E+12	5.69E+12	3.68E+12	4.05E+12
Standard Deviation	8.00E+12	1.89E+12	6.34E+12	3.36E+12	1.80E+12	1.17E+12	1.39E+12	1.12E+12	2.93E+11
95% Confidence Interval	9.93E+12	2.34E+12	7.88E+12	4.17E+12	2.24E+12	1.45E+12	1.73E+12	1.39E+12	3.64E+11
CI Upper limit	3.28E+13	8.77E+12	2.62E+13	1.93E+13	9.17E+12	6.54E+12	7.42E+12	5.07E+12	4.41E+12
CI Lower limit	1.29E+13	4.09E+12	1.05E+13	1.10E+13	4.69E+12	3.65E+12	3.96E+12	2.29E+12	3.69E+12
Sample	**9**	**10**	**11**	**12**	**13**	**14**			
Carbon content (%)	20	40	40	60	60	60			
Measurements	8.58E+10	3.77E+08	6.50E+08	6.11E+06	6.16E+06	1.28E+06			
	1.66E+11	8.47E+08	6.52E+08	5.83E+06	5.92E+06	1.31E+06			
	3.75E+11	7.16E+08	1.63E+08	5.76E+06	8.01E+06	1.46E+06			
	8.95E+11	6.53E+08	5.17E+08	8.44E+06	8.42E+06	1.43E+06			
	7.00E+11	2.70E+08	6.70E+08	9.19E+06	3.17E+06	1.42E+06			
Surface Resistivity ρs (Ω)	4.44E+11	5.73E+08	5.30E+08	7.07E+06	6.34E+06	1.38E+06			
Standard Deviation	3.46E+11	2.41E+08	2.14E+08	1.62E+06	2.08E+06	8.03E+04			
95% Confidence Interval	4.30E+11	2.99E+08	2.66E+08	2.02E+06	2.59E+06	9.98E+04			
CI Upper limit	8.74E+11	8.72E+08	7.97E+08	9.08E+06	8.92E+06	1.48E+06			
CI Lower limit	1.44E+10	2.74E+08	2.64E+08	5.05E+06	3.75E+06	1.28E+06			

Table 10: Volume electrical resistivity of samples as listed in table 7

Sample	**Untreated**	**1**	**2**	**3**	**4**	**5**	**6**	**7**	**8**
Carbon content (%)	no coating	0	1	2	3	5	5	7	10
Measurements	8.74E+14	5.50E+14	1.43E+14	2.04E+14	7.35E+13	8.62E+13	1.74E+14	8.45E+13	1.42E+14
	4.68E+14	4.89E+14	2.23E+14	2.19E+14	9.68E+13	1.20E+13	1.42E+14	7.97E+13	1.33E+14
	9.11E+14	3.17E+14	1.74E+14	1.86E+14	7.08E+13	8.30E+13	1.59E+14	8.19E+13	1.72E+14
	2.40E+14	3.10E+14	2.53E+14	1.76E+14	1.02E+14	8.65E+13	1.45E+14	8.19E+13	1.27E+14
	1.50E+14	2.92E+14	1.73E+14	1.86E+14	1.45E+14	7.64E+13	1.68E+14	9.05E+13	1.45E+14
Volume Resistivity ρv (Ω.cm)	5.28E+14	3.91E+14	1.93E+14	1.94E+14	9.76E+13	6.88E+13	1.58E+14	8.37E+13	1.44E+14
Standard Deviation	3.52E+14	1.19E+14	4.43E+13	1.73E+13	2.99E+13	3.20E+13	1.38E+13	4.14E+12	1.73E+13
95% confidence interval	4.37E+14	1.48E+14	5.50E+13	2.15E+13	3.71E+13	3.98E+13	1.72E+13	5.15E+12	2.15E+13
CI Upper limit	9.65E+14	5.40E+14	2.48E+14	2.16E+14	1.35E+14	1.09E+14	1.75E+14	8.89E+13	1.66E+14
CI Lower limit	9.13E+13	2.43E+14	1.38E+14	1.73E+14	6.05E+13	2.91E+13	1.41E+14	7.86E+13	1.23E+14
Sample	**9**	**10**	**11**	**12**	**13**	**14**			
Carbon content (%)	20	40	40	60	60	60			
Measurements	8.27E+12	3.15E+10	1.12E+10	5.56E+08	7.65E+08	1.28E+08			
	2.03E+13	2.95E+10	1.14E+10	5.24E+08	6.89E+09	1.31E+08			
	4.59E+13	2.86E+10	1.39E+10	5.46E+08	8.62E+08	1.46E+08			
	7.73E+13	2.88E+10	1.73E+10	2.47E+08	6.92E+09	1.43E+08			
	5.64E+13	3.04E+10	1.76E+10	2.05E+08	7.61E+09	1.42E+08			
Volume Resistivity ρv (Ω.cm)	4.16E+13	2.97E+10	1.43E+10	4.16E+08	4.61E+09	1.38E+08			
Standard Deviation	2.77E+13	1.22E+09	3.09E+09	1.74E+08	3.48E+09	8.03E+06			
95% confidence interval	3.44E+13	1.51E+09	3.83E+09	2.16E+08	4.32E+09	9.98E+06			
CI Upper limit	7.60E+13	3.13E+10	1.81E+10	6.32E+08	8.93E+09	1.48E+08			
CI Lower limit	7.19E+12	2.82E+10	1.05E+10	2.00E+08	2.91E+08	1.28E+08			

Carbon powder electrical resistivity data analysis

	Graphene electrical volume resistivity (Ω.cm)	***Sphericle graphite electrical volume resistivity (Ω.cm)***
Mean	10.21	13.13
Standard Error	0.78	0.15
Median	9.03	13.07
Mode	#N/A	#N/A
Standard Deviation	1.74	0.33
Sample Variance	3.03	0.11
Kurtosis	-2.67	-0.27
Skewness	0.72	0.72
Range	3.57	0.83
Minimum	8.91	12.78
Maximum	12.49	13.61
Sum	51.07	65.67
Count	5.00	5.00
Confidence Level(95.0%)	2.16	0.41

Surface electrical resistivity data analysis

Untreated		*Sample 1*		*Sample 2*		*Sample 3*	
Mean	2.29E+13	Mean	6.43E+12	Mean	1.83E+13	Mean	1.52E+13
Standard Error	3.58E+12	Standard Error	8.44E+11	Standard Error	2.84E+12	Standard Error	1.50E+12
Median	2.20E+13	Median	5.59E+12	Median	1.80E+13	Median	1.39E+13
Mode	#N/A	Mode	#N/A	Mode	#N/A	Mode	#N/A
Standard Deviation	8.00E+12	Standard Deviation	1.89E+12	Standard Deviation	6.34E+12	Standard Deviation	3.36E+12
Sample Variance	6.40E+25	Sample Variance	3.56E+24	Sample Variance	4.02E+25	Sample Variance	1.13E+25
Kurtosis	-1.09E+00	Kurtosis	4.74E+00	Kurtosis	-2.80E+00	Kurtosis	3.58E+00
Skewness	5.88E-01	Skewness	2.17E+00	Skewness	1.54E-02	Skewness	1.87E+00
Range	1.87E+13	Range	4.37E+12	Range	1.36E+13	Range	8.23E+12
Minimum	1.55E+13	Minimum	5.42E+12	Minimum	1.12E+13	Minimum	1.27E+13
Maximum	3.42E+13	Maximum	9.78E+12	Maximum	2.48E+13	Maximum	2.10E+13
Sum	1.14E+14	Sum	3.22E+13	Sum	9.16E+13	Sum	7.58E+13
Count	5.00E+00	Count	5.00E+00	Count	5.00E+00	Count	5.00E+00
Confidence Level(95.0%)	9.93E+12	Confidence Level(95.0%)	2.34E+12	Confidence Level(95.0%)	7.88E+12	Confidence Level(95.0%)	4.17E+12

Sample 4		*Sample5*		*Sample 6*		*Sample 7*	
Mean	6.93E+12	Mean	5.09E+12	Mean	5.69E+12	Mean	3.68E+12
Standard Error	8.07E+11	Standard Error	5.22E+11	Standard Error	6.24E+11	Standard Error	5.01E+11
Median	6.24E+12	Median	5.40E+12	Median	5.27E+12	Median	3.07E+12
Mode	#N/A	Mode	#N/A	Mode	#N/A	Mode	#N/A
Standard Deviation	1.80E+12	Standard Deviation	1.17E+12	Standard Deviation	1.39E+12	Standard Deviation	1.12E+12
Sample Variance	3.26E+24	Sample Variance	1.36E+24	Sample Variance	1.94E+24	Sample Variance	1.26E+24
Kurtosis	-1.89E+00	Kurtosis	1.48E+00	Kurtosis	2.54E+00	Kurtosis	1.28E-01
Skewness	6.68E-01	Skewness	-1.06E+00	Skewness	1.58E+00	Skewness	1.15E+00
Range	4.13E+12	Range	3.10E+12	Range	3.49E+12	Range	2.70E+12
Minimum	5.26E+12	Minimum	3.26E+12	Minimum	4.53E+12	Minimum	2.71E+12
Maximum	9.39E+12	Maximum	6.35E+12	Maximum	8.02E+12	Maximum	5.41E+12
Sum	3.46E+13	Sum	2.55E+13	Sum	2.85E+13	Sum	1.84E+13
Count	5.00E+00	Count	5.00E+00	Count	5.00E+00	Count	5.00E+00
Confidence Level(95.0%)	2.24E+12	Confidence Level(95.0%)	1.45E+12	Confidence Level(95.0%)	1.73E+12	Confidence Level(95.0%)	1.39E+12

Sample 8		*Sample 9*		*Sample 10*		*Sample 11*	
Mean	4.05E+12	Mean	4.44E+11	Mean	5.73E+08	Mean	5.30E+08
Standard Error	1.31E+11	Standard Error	1.55E+11	Standard Error	1.08E+08	Standard Error	9.59E+07
Median	3.93E+12	Median	3.75E+11	Median	6.53E+08	Median	6.50E+08
Mode	#N/A	Mode	#N/A	Mode	#N/A	Mode	#N/A
Standard Deviation	2.93E+11	Standard Deviation	3.46E+11	Standard Deviation	2.41E+08	Standard Deviation	2.14E+08
Sample Variance	8.57E+22	Sample Variance	1.20E+23	Sample Variance	5.81E+16	Sample Variance	4.60E+16
Kurtosis	3.46E+00	Kurtosis	-2.07E+00	Kurtosis	-2.07E+00	Kurtosis	3.26E+00
Skewness	1.84E+00	Skewness	4.05E-01	Skewness	-3.30E-01	Skewness	-1.83E+00
Range	7.13E+11	Range	8.10E+11	Range	5.77E+08	Range	5.07E+08
Minimum	3.84E+12	Minimum	8.58E+10	Minimum	2.70E+08	Minimum	1.63E+08
Maximum	4.55E+12	Maximum	8.95E+11	Maximum	8.47E+08	Maximum	6.70E+08
Sum	2.02E+13	Sum	2.22E+12	Sum	2.86E+09	Sum	2.65E+09
Count	5.00E+00	Count	5.00E+00	Count	5.00E+00	Count	5.00E+00
Confidence Level(95.0%)	3.64E+11	Confidence Level(95.0%)	4.30E+11	Confidence Level(95.0%)	2.99E+08	Confidence Level(95.0%)	2.66E+08

Sample 12		*Sample 13*		*Sample 14*	
Mean	7.07E+06	Mean	6.34E+06	Mean	1.38E+06
Standard Error	7.26E+05	Standard Error	9.32E+05	Standard Error	3.59E+04
Median	6.11E+06	Median	6.16E+06	Median	1.42E+06
Mode	#N/A	Mode	#N/A	Mode	#N/A
Standard Deviation	1.62E+06	Standard Deviation	2.08E+06	Standard Deviation	8.03E+04
Sample Variance	2.63E+12	Sample Variance	4.34E+12	Sample Variance	6.46E+09
Kurtosis	-2.61E+00	Kurtosis	4.33E-01	Kurtosis	-2.77E+00
Skewness	6.97E-01	Skewness	-8.34E-01	Skewness	-4.80E-01
Range	3.43E+06	Range	5.25E+06	Range	1.79E+05
Minimum	5.76E+06	Minimum	3.17E+06	Minimum	1.28E+06
Maximum	9.19E+06	Maximum	8.42E+06	Maximum	1.46E+06
Sum	3.53E+07	Sum	3.17E+07	Sum	6.89E+06
Count	5.00E+00	Count	5.00E+00	Count	5.00E+00
Confidence Level(95.0%)	2.02E+06	Confidence Level(95.0%)	2.59E+06	Confidence Level(95.0%)	9.98E+04

Volume electrical resistivity data analysis

Untreated		*Sample 1*		*Sample 2*		*Sample 3*	
Mean	5.28E+14	Mean	3.91E+14	Mean	1.93E+14	Mean	1.94E+14
Standard Error	1.57E+14	Standard Error	5.34E+13	Standard Error	1.98E+13	Standard Error	7.76E+12
Median	4.68E+14	Median	3.17E+14	Median	1.74E+14	Median	1.86E+14
Mode	#N/A	Mode	#N/A	Mode	#N/A	Mode	#N/A
Standard Deviation	3.52E+14	Standard Deviation	1.19E+14	Standard Deviation	4.43E+13	Standard Deviation	1.73E+13
Sample Variance	1.24E+29	Sample Variance	1.42E+28	Sample Variance	1.96E+27	Sample Variance	3.01E+26
Kurtosis	-2.87E+00	Kurtosis	-2.43E+00	Kurtosis	-1.25E+00	Kurtosis	-6.56E-01
Skewness	1.78E-01	Skewness	7.32E-01	Skewness	4.68E-01	Skewness	7.89E-01
Range	7.61E+14	Range	2.59E+14	Range	1.11E+14	Range	4.33E+13
Minimum	1.50E+14	Minimum	2.92E+14	Minimum	1.43E+14	Minimum	1.76E+14
Maximum	9.11E+14	Maximum	5.50E+14	Maximum	2.53E+14	Maximum	2.19E+14
Sum	2.64E+15	Sum	1.96E+15	Sum	9.67E+14	Sum	9.70E+14
Count	5.00E+00	Count	5.00E+00	Count	5.00E+00	Count	5.00E+00
Confidence Level(95.0%)	4.37E+14	Confidence Level(95.0%)	1.48E+14	Confidence Level(95.0%)	5.50E+13	Confidence Level(95.0%)	2.15E+13

Sample 4		*Sample5*		*Sample 6*		*Sample 7*	
Mean	9.76E+13	Mean	6.88E+13	Mean	1.58E+14	Mean	8.37E+13
Standard Error	1.34E+13	Standard Error	1.43E+13	Standard Error	6.19E+12	Standard Error	1.85E+12
Median	9.68E+13	Median	8.30E+13	Median	1.59E+14	Median	8.19E+13
Mode	#N/A	Mode	#N/A	Mode	#N/A	Mode	8.19E+13
Standard Deviation	2.99E+13	Standard Deviation	3.20E+13	Standard Deviation	1.38E+13	Standard Deviation	4.14E+12
Sample Variance	8.92E+26	Sample Variance	1.03E+27	Sample Variance	1.92E+26	Sample Variance	1.72E+25
Kurtosis	1.26E+00	Kurtosis	4.67E+00	Kurtosis	-2.61E+00	Kurtosis	2.05E+00
Skewness	1.14E+00	Skewness	-2.15E+00	Skewness	-6.93E-02	Skewness	1.37E+00
Range	7.42E+13	Range	7.45E+13	Range	3.12E+13	Range	1.08E+13
Minimum	7.08E+13	Minimum	1.20E+13	Minimum	1.42E+14	Minimum	7.97E+13
Maximum	1.45E+14	Maximum	8.65E+13	Maximum	1.74E+14	Maximum	9.05E+13
Sum	4.88E+14	Sum	3.44E+14	Sum	7.89E+14	Sum	4.19E+14
Count	5.00E+00	Count	5.00E+00	Count	5.00E+00	Count	5.00E+00
Confidence Level(95.0%)	3.71E+13	Confidence Level(95.0%)	3.98E+13	Confidence Level(95.0%)	1.72E+13	Confidence Level(95.0%)	5.15E+12

Sample 8		*Sample 9*		*Sample 10*		*Sample 11*	
Mean	1.44E+14	Mean	4.16E+13	Mean	2.97E+10	Mean	1.43E+10
Standard Error	7.75E+12	Standard Error	1.24E+13	Standard Error	5.43E+08	Standard Error	1.38E+09
Median	1.42E+14	Median	4.59E+13	Median	2.95E+10	Median	1.39E+10
Mode	#N/A	Mode	#N/A	Mode	#N/A	Mode	#N/A
Standard Deviation	1.73E+13	Standard Deviation	2.77E+13	Standard Deviation	1.22E+09	Standard Deviation	3.09E+09
Sample Variance	3.01E+26	Sample Variance	7.69E+26	Sample Variance	1.48E+18	Sample Variance	9.52E+18
Kurtosis	2.19E+00	Kurtosis	-1.43E+00	Kurtosis	-5.43E-01	Kurtosis	-3.00E+00
Skewness	1.35E+00	Skewness	3.53E-02	Skewness	8.12E-01	Skewness	1.72E-01
Range	4.50E+13	Range	6.90E+13	Range	2.93E+09	Range	6.37E+09
Minimum	1.27E+14	Minimum	8.27E+12	Minimum	2.86E+10	Minimum	1.12E+10
Maximum	1.72E+14	Maximum	7.73E+13	Maximum	3.15E+10	Maximum	1.76E+10
Sum	7.20E+14	Sum	2.08E+14	Sum	1.49E+11	Sum	7.15E+10
Count	5.00E+00	Count	5.00E+00	Count	5.00E+00	Count	5.00E+00
Confidence Level(95.0%)	2.15E+13	Confidence Level(95.0%)	3.44E+13	Confidence Level(95.0%)	1.51E+09	Confidence Level(95.0%)	3.83E+09

Sample 12		*Sample 13*		*Sample 14*	
Mean	4.16E+08	Mean	4.61E+09	Mean	1.38E+08
Standard Error	7.79E+07	Standard Error	1.56E+09	Standard Error	3.59E+06
Median	5.24E+08	Median	6.89E+09	Median	1.42E+08
Mode	#N/A	Mode	#N/A	Mode	#N/A
Standard Deviation	1.74E+08	Standard Deviation	3.48E+09	Standard Deviation	8.03E+06
Sample Variance	3.03E+16	Sample Variance	1.21E+19	Sample Variance	6.46E+13
Kurtosis	-3.11E+00	Kurtosis	-3.28E+00	Kurtosis	-2.77E+00
Skewness	-6.21E-01	Skewness	-5.77E-01	Skewness	-4.80E-01
Range	3.51E+08	Range	6.85E+09	Range	1.79E+07
Minimum	2.05E+08	Minimum	7.65E+08	Minimum	1.28E+08
Maximum	5.56E+08	Maximum	7.61E+09	Maximum	1.46E+08
Sum	2.08E+09	Sum	2.31E+10	Sum	6.89E+08
Count	5.00E+00	Count	5.00E+00	Count	5.00E+00
Confidence Level(95.0%)	2.16E+08	Confidence Level(95.0%)	4.32E+09	Confidence Level(95.0%)	9.98E+06